ai_at_1[1].pdf

Delhi Technological University

Document Details

Submission ID
trn:oid:::27535:100008730

Submission Date
Jun 9, 2025, 3:35 PM GMT+5:30

Download Date
Jun 9, 2025, 3:37 PM GMT+5:30

File Name
ai_at_1[1].pdf

File Size
1.7 MB

54 Pages

11,624 Words

70,168 Characters

7% Overall Similarity

The combined total of all matches, including overlapping sources, for each database.

Filtered from the Report

- Bibliography
- Quoted Text
- Cited Text
- Small Matches (less than 8 words)

Match Groups

89 Not Cited or Quoted 7%
Matches with neither in-text citation nor quotation marks

0 Missing Quotations 0%
Matches that are still very similar to source material

0 Missing Citation 0%
Matches that have quotation marks, but no in-text citation

0 Cited and Quoted 0%
Matches with in-text citation present, but no quotation marks

Top Sources

4% Internet sources
4% Publications
6% Submitted works (Student Papers)

Integrity Flags

0 Integrity Flags for Review

No suspicious text manipulations found.

Our system's algorithms look deeply at a document for any inconsistencies that would set it apart from a normal submission. If we notice something strange, we flag it for you to review.

A Flag is not necessarily an indicator of a problem. However, we'd recommend you focus your attention there for further review.

Match Groups

- **89** Not Cited or Quoted 7%
  Matches with neither in-text citation nor quotation marks
- **0** Missing Quotations 0%
  Matches that are still very similar to source material
- **0** Missing Citation 0%
  Matches that have quotation marks, but no in-text citation
- **0** Cited and Quoted 0%
  Matches with in-text citation present, but no quotation marks

Top Sources

- 4% Internet sources
- 4% Publications
- 6% Submitted works (Student Papers)

Top Sources

The sources with the highest number of matches within the submission. Overlapping sources will not be displayed.

1	Internet	
www.science.gov		<1%
2	Internet	
iopscience.iop.org		<1%
3	Internet	
www.ncbi.nlm.nih.gov		<1%
4	Internet	
d.docksci.com		<1%
5	Submitted works	
Higher Education Commission Pakistan on 2025-01-30		<1%
6	Submitted works	
University College London on 2023-09-01		<1%
7	Submitted works	
Higher Education Commission Pakistan on 2016-01-04		<1%
8	Submitted works	
VIT University on 2025-03-21		<1%
9	Publication	
John R. Reynolds, Barry C. Thompson, Terje A. Skotheim. "Conjugated Polymers - ...		<1%
10	Publication	
Shams u Zaman, Junaid Riaz, Ihtesham Ghani, Amina Bibi, Muhammad Arif. "DFT-...		<1%

11 Publication
Trinh T.M. Vo, Andrew J. Williamson, Vincenzo Lordi, Giulia Galli. "Atomistic Desig... <1%

12 Publication
Liu, Yu. "Thermoelectric Properties of Metal Sulfide Ceramics and Thin Films", The... <1%

13 Publication
Xiao-Lei Shi, Jin Zou, Zhi-Gang Chen. "Advanced Thermoelectric Design: From Mat... <1%

14 Submitted works
University College London on 2020-01-27 <1%

15 Submitted works
Yonsei University on 2024-12-16 <1%

16 Internet
www.researchsquare.com <1%

17 Internet
www.spiedigitallibrary.org <1%

18 Submitted works
La Trobe University on 2018-03-05 <1%

19 Internet
materialsmodeling.org <1%

20 Submitted works
Dong Nai Technology University on 2025-05-06 <1%

21 Submitted works
Indian Institute of Science Education and Research on 2023-05-29 <1%

22 Internet
www.nature.com <1%

23 Internet
www.rlmm.org <1%

24 Submitted works
Gauhati University on 2014-10-24 <1%

25 Submitted works
Higher Education Commission Pakistan on 2025-05-11 <1%

26 Internet
escholarship.org <1%

27 Publication
Harsha Verma, Manwendra K. Tripathi, Mohan L. Verma. "Structural, electronic, t... <1%

28 Submitted works
Indian Institute of Technology on 2016-05-05 <1%

29 Submitted works
Johns Hopkins Unversity on 2024-09-14 <1%

30 Publication
Okoye, C.M.I.. "Ab initio study of structural, electronic and optical properties of ... <1%

31 Submitted works
University of Edinburgh on 2015-03-15 <1%

32 Publication
Xiaotong Li, Boubacar Traoré, Mikaël Kepenekian, Linda Li et al. "Bismuth/Silver-... <1%

33 Internet
num.univ-msila.dz <1%

34 Internet
www.researchgate.net <1%

35 Internet
www.sigaa.ufs.br <1%

36 Publication
Annalise E. Maughan, Alex M. Ganose, David O. Scanlon, James R. Neilson. "Persp... <1%

37 Publication
Fairuz Izzuddin Romli, Salim Mkubwa Salim. "Preliminary Study of Passengers' Bo... <1%

38 Submitted works
Higher Education Commission Pakistan on 2012-11-06 <1%

39 Submitted works
Indian Institute of Technology on 2016-08-26 <1%

40 Publication
Jie Chen, Hai L. Feng, Kazunari Yamaura. "Review of progress in the materials dev... <1%

41 Submitted works
King Abdullah University of Science and Technology (KAUST) on 2023-01-01 <1%

42 Submitted works
The University of Tokyo on 2024-01-14 <1%

43 Submitted works
University College London on 2024-08-21 <1%

44 Submitted works
University of Newcastle upon Tyne on 2013-11-07 <1%

45 Submitted works
University of St Andrews on 2024-07-25 <1%

46 Internet
digitalcommons.usf.edu <1%

47 Publication
Akinobu Nakada, Masanobu Higashi, Takuma Kimura, Hajime Suzuki et al. "Band ... <1%

48 Publication
G. Brillant, A. Pasturel. " Study of Ba and Zr stability in by density functional calcu... <1%

49 Submitted works
Jawaharlal Nehru Technological University on 2024-11-02 <1%

50 Publication
Jin, Jianbo. "Study of Halide Perovskites at the Level of Ionic Octahedron", Univer... <1%

51 Publication
Mehvish Fatima, Sikander Azam, Mahpara Ghazanfar, Shagufta Rasool et al. "Firs... <1%

52 Publication
Quinten A. Akkerman, Liberato Manna. "What Defines a Halide Perovskite?", ACS ... <1%

53	Publication	Shrikaant Kulkarni, Vipul Srivastava, P. William. "Contemporary Advancements in ... <1%
54	Submitted works	The University of Manchester on 2025-04-04 <1%
55	Submitted works	Universiti Malaysia Sabah on 2024-09-05 <1%
56	Submitted works	University of Birmingham on 2025-03-20 <1%
57	Submitted works	University of Durham on 2009-04-29 <1%
58	Submitted works	University of Surrey on 2015-11-09 <1%
59	Publication	Yu Wu, Junbo He, Ying Chen, Mingran Kong, Yiming Zhang, Xiaobing Hu, Jianwei L... <1%
60	Internet	dlib.hust.edu.vn:8080 <1%
61	Internet	jmol.sourceforge.net <1%
62	Internet	journals.iucr.org <1%
63	Internet	link.springer.com <1%
64	Internet	mdpi-res.com <1%
65	Internet	mrs.org <1%
66	Internet	oaepublishstorage.blob.core.windows.net <1%

67 Internet

rmf.smf.mx <1%

CHAPTER 1

INTRODUCTION

1. Introduction and Motivation

The growing urgency to develop clean and efficient energy technologies has intensified the search for materials capable of converting waste heat into electricityan attribute central to thermoelectric (TE) materials. These materials provide a solid-state, environmentally friendly solution for energy recovery, with practical applications in automotive and industrial waste heat harvesting, portable and wearable electronics, aerospace, and climate control systems.

Among the broad landscape of thermoelectric candidates, **lead-free perovskite oxides** stand out due to their **inherent low lattice thermal conductivity**, **excellent thermal stability**, and **highly tunable electronic properties**. The classic **ABX_3 perovskite crystal structure** is structurally versatile, supporting a wide range of elemental substitutions at both A and B sites. This flexibility not only accommodates diverse chemistries but also enables precise optimization of electrical and thermal transport properties, making perovskites ideal candidates for energy conversion technologies.

Perovskites are already at the forefront of several advanced technologies. **Halide perovskites** have revolutionized the field of photovoltaics, with certified power conversion efficiencies now exceeding 25%, while **oxide perovskites** are widely applied in solid oxide fuel cells, sensors, ferroelectric memory devices, and superconductors. These wide-ranging applications stem from the **multi-functional nature of the perovskite lattice**, which supports phenomena such as ferroelectricity, ionic conductivity, magnetoresistance, and multiferroicity.

2. Focus of the Study

This thesis focuses on the computational evaluation of two **lead-free cubic perovskite oxidesLiGeCl$_3$** and **CuLuO$_3$**, both crystallizing in the highly symmetric **Pm-3m space group (#221)**. These compounds were selected based on their structural simplicity, band gap characteristics, and potential for high thermoelectric performance.

To assess their viability as thermoelectric materials, we employ a combination of **Density Functional Theory (DFT)** and **Boltzmann Transport Theory** to compute essential performance indicators such as the **Seebeck coefficient**, **power factor**, and **dimensionless figure of merit (ZT)**. Additionally, we review structural stability across a broader set of perovskite oxides by analyzing **phonon dispersion**, **Goldschmidt tolerance factors**, and their **thermal response under varying temperatures**.

This study not only evaluates the **intrinsic electronic transport properties** of $LiGeCl_3$ and $CuLuO_3$ but also integrates them into a broader framework aimed at identifying **thermoelectrically efficient and structurally stable perovskite materials**. Our findings contribute to the ongoing development of **non-toxic, high-performance thermoelectric materials** suited for real-world energy applications.

3. Historical and Structural Context of Perovskites

The term "perovskite" originates from the mineral **$CaTiO_3$**, discovered in 1839 by Gustav Rose and named after Russian mineralogist **Lev Perovski**. The perovskite structure has since evolved into a vast family of compounds with the general formula **ABX_3**, where A is a larger cation located at the cube corners and B is a smaller cation octahedrally coordinated by anions X (typically oxygen or halogens).

What makes perovskites remarkable is their **structural adaptability**. Over the decades, numerous oxides, halides, and mixed-metal variants have been synthesized, many of which are classified by their **Goldschmidt tolerance factor**, a measure of their geometric stability. This adaptability has given rise to a wide range of functionalities across **optics, electronics, magnetism, and energy storage**.

4. Advances in Thermoelectric Perovskites

Traditionally, high-performance thermoelectrics have relied on toxic and air-sensitive compounds like **PbTe** and **Bi_2Te_3**. In contrast, **oxide perovskites** such as **$SrTiO_3$** and **$CaMnO_3$**, especially when doped with aliovalent ions (e.g., Nb), have shown promise in high-temperature TE applications. For example, **Nb-doped $SrTiO_3$** has reached **ZT ≈ 0.37** near 1000 K. However, high thermal conductivity remains a bottleneck.

Recent work has shifted toward lead-free halide perovskites and double perovskites like $Cs_2AgBiBr_6$, which demonstrate ultra-low lattice thermal conductivities due to strong anharmonic phonon scattering. Similarly, high-entropy perovskite oxides, 2D layered variants, and vacancy-engineered structures are being explored to further enhance TE efficiency.

While halide perovskites face stability challenges, oxide perovskites remain robust at high temperatures, making them suitable for waste-heat recovery systems operating in oxidative environments.

5. Environmental and Technological Relevance

Thermoelectric systems offer a sustainable approach to reducing global energy waste. A significant proportion of energy generated across sectors is lost as heat; TE devices can partially reclaim this energy, reducing overall emissions. Importantly, **lead-free oxide perovskites**including $LiGeCl_3$ and $CuLuO_3$do not contain hazardous elements, making them environmentally safe and scalable.

Their chemical durability, air stability, and high-temperature resilience position them as strong candidates for next-generation TE devices. As materials science increasingly prioritizes eco-friendly and cost-effective solutions, the advancement of such compounds is both timely and essential.

Literature review

Types of perovskites

Perovskite materials, with the general formula ABX_3, are highly adaptable compounds known for their unique structural and functional properties. Their flexible framework allows for tuning characteristics for various applications, from solar cells to catalysis. This review explores key perovskite types, their structures, synthesis methods, and emerging uses, showing their potential as next-generation functional materials. 1, 2

Hybrid Organic-Inorganic Halide Perovskites

Halide perovskites, especially in solar technology, have gained major attention for their high power conversion efficienciesover 26.7% for single-junction and 34.7% for tandem cells 3. These hybrid materials, typically with the ABX_3 structure (A = MA/FA/Cs, B = Pb/Sn, X = I/Br/Cl), offer excellent optoelectronic properties and tunable bandgaps 1. Mixed-halide variants allow precise control over absorption and charge transport. Recent advancements, such as those by CubicPV, have improved stability, accelerating commercialization. The global perovskite solar market is projected to grow from $94.8 million in 2022 to $2.48 billion by 2032All-Inorganic Halide Perovskites 5, 6

All-inorganic halide perovskites

like $CsPbI_3$ and $CsPbBr_3$ offer better thermal stability than hybrid types, as they lack volatile organic components. This makes them ideal for high-temperature and long-term applications 6. While achieving stable phases requires precise synthesis, once stabilized, they perform well under harsh conditions. Computational tools have also accelerated their discovery and optimization for photovoltaic and other demanding uses. 7

Two-Dimensional Layered Perovskites

Two-dimensional (2D) perovskites, derived from the structural reduction of 3D frameworks, exhibit enhanced environmental stability and quantum confinement effects, which influence their charge and heat transportkey factors in thermoelectric performance. E.g., Ruddlesden–Popper, Dion–Jacobson

Halide Layered Double Perovskites (LDPs)

Halide layered double perovskites (LDPs) expand the perovskite family by enabling the incorporation of multiple metal cations with different oxidation states. These follow the formulas $(A)_4B^iB^{ii}X_8$ or $(A)_2A'B^iB^{ii}X_7$, where B^i and B^{ii} are metals in distinct oxidation states 8. The reduced dimensionality permits the synthesis of materials not feasible in bulk form due to octahedral size mismatches.

LDPs allow significant compositional flexibility, enabling fine-tuning of electronic and thermal properties through quantum confinement effects 8. Most known LDPs are single-layered (n = 1), with a few double-layered (n = 2) forms synthesized using cesium as the A-site cation. E.g., $Cs_2AgBiBr_6$

Single Perovskite Oxides (ABO_3)

Oxide perovskites with the ABO_3 structure are widely studied for applications in catalysis, energy storage, and sensing. They consist of A-site cations (typically alkaline earth or rare earth metals) and B-site transition metals, forming a 3D network of BO_6 octahedra 3 , 10.

Recent studies highlight their potential in energy storage due to oxygen anion-intercalation mechanisms. Their oxygen vacancies and structural flexibility make them promising for pseudocapacitive behaviour in supercapacitors 2, 12. Furthermore, substitution at A and B sites allows for precise tuning of electronic properties, relevant to thermoelectric performance.

These materials are also effective for gas sensing due to their redox activity, electronic mobility, and structural stability. The coexistence of cationic and oxygen vacancies enhances their sensitivity to gases like NO_2, CO, H_2, and VOCs. E.g., $SrTiO_3$, $LaFeO_3$

Double Perovskite Oxides ($A_2BB'O_6$)

Double oxide perovskites ($A_2BB'O_6$) incorporate two different B-site cations, leading to various ordered structures such as rock-salt, layered, or columnar patternseach influencing the material's properties 13,.

They have shown promise for oxygen evolution reaction (OER) electrocatalysis and energy storage, offering precise control over oxygen vacancy concentration, conductivity, and surface activity 13. Recent theoretical and experimental studies have deepened understanding of their catalytic and charge transport behavior, pointing to their potential in thermoelectric applications.

Single Atom–Perovskite Composite Materials (SA-PCs)

A promising development in perovskite research is the integration of single-atom catalysts (SACs) with perovskite supports, forming single atom–perovskite composites (SA-PCs). These materials combine the catalytic efficiency of SACs with the structural tunability and electronic properties of perovskites.

SA-PCs are typically synthesized via wet impregnation, atomic layer deposition, or in-situ growth methods. Their atomic dispersion and metal-support interactions are studied using advanced characterization tools like HR-TEM, XAS, and STEM. These composites show improved charge separation and transport, along with high thermal and structural stabilitytraits beneficial for thermoelectric and catalytic applications 14.

Vacancy-Ordered and Anti-Perovskites

New classes such as vacancy-ordered perovskites (e.g., A_2BX_6, $A_3B_2X_9$) and anti-perovskites (where halides occupy cation sites) offer unique structural and electronic behaviors 12, 16. The introduction of A- or B-site vacancies allows tuning of band structures and stabilization of unusual oxidation states, relevant for enhancing thermoelectric properties.

ReO_3-Type Structures

ReO_3-type compounds (BX_3) can be viewed as perovskites with vacant A-sites . These materials feature open frameworks that enable negative thermal expansion, high electronic mobility, and photocatalytic activity. Their unique transport and structural behaviors make them potential candidates for future thermoelectric materials.

Complex Perovskite Structures

Complex perovskites with ordered cations on A and B sitessuch as Aurivillius, Dion–Jacobson, and Ruddlesden–Popper phasesexpand the design space of perovskites 8. Their layered architecture and mixed valency allow tailored electronic and thermal properties, making them attractive for energy conversion applications, including thermoelectric. Aurivillius, Dion–Jacobson, Ruddlesden–Popper

Role of Perovskites in Thermoelectric Materials

Perovskite materials have emerged as promising candidates for thermoelectric energy conversion due to their exceptional structural versatility, tunable electronic properties, and intrinsically low thermal conductivity. This review examines the thermoelectric performance of halide, oxide, and double perovskite variants, focusing on the interplay between their electronic structures, charge transport mechanisms, and lattice dynamics. Key advancements in doping strategies, nanostructuring, and composite engineering are analyzed to elucidate pathways for optimizing the dimensionless figure of merit (ZT), with recent breakthroughs achieving ZT values up to 1.52 in doped oxide perovskites and 0.96 in double perovskites. Challenges in stability, scalability, and performance

consistency are critically assessed, providing a roadmap for future research in this rapidly evolving field.

Structural and Electronic Foundations of Perovskite Thermoelectric

The perovskite crystal structure (ABX_3) enables unparalleled flexibility in tailoring thermoelectric properties through cationic/anionic substitutions and dimensional engineering. The corner-sharing BX_6 octahedra framework accommodates a wide range of A-site cations (e.g., Cs^+, MA^+, Ba^{2+}) and B-site transition metals (e.g., Sn^{2+}, Pb^{2+}, Mn^{3+}), allowing precise control over bandgap, carrier concentration, and phonon scattering mechanisms 2. For thermoelectric, this structural adaptability permits simultaneous optimization of the Seebeck coefficient (α), electrical conductivity (σ), and thermal conductivity (κ)parameters governed by the **Pisarenko relation** and **Wiedemann-Franz law**.

Halide Perovskites: Balancing Low Thermal Conductivity and Charge Mobility

Hybrid Organic-Inorganic Halides

Methylammonium lead iodide ($MAPbI_3$) exhibits ultra-low lattice thermal conductivity (0.3–0.42 W/m·K) due to anharmonic phonon scattering from organic cation rattling and soft Pb-I bonds 20. Single-crystal $MAPbI_3$ achieves remarkable α values of 920 μV/K at 297 K, though low σ (~10^{-5} S/cm) limits ZT to ~0.07 21 22. Chlorine doping (e.g., $MAPbI_{3-x}Cl_x$) enhances stability and σ by introducing shallow defect states, while mixed halide compositions (I/Br/Cl) enable bandgap tuning for optimal α 21 24.

All-Inorganic Halides

Cesium-based halides like $Cs_2Au(I)Au(III)I_6$ demonstrate superior thermal stability and a unique 2D electronic structure, yielding high in-plane power factors ($\alpha^2\sigma$) of 1.5 mW/m·K² at 300 K2. Theoretical studies predict $ZT \approx 1$ at 300 K and ≈4 at 800 K for $Cs_2Au(I)Au(III)I_6$, driven by low κ (0.5 W/m·K) and degenerate carrier concentrations

25. However, experimental *ZT* values remain below 0.2 due to oxidation challenges and interfacial defects21

Oxide Perovskites: Stability and High-Temperature Performance

Single Perovskite Oxides

13 $BaSnO_3$ exhibits outstanding dynamic stability and a high *ZT* of 1.52 at 900 K for p-type doping, attributed to its high α (−350 μV/K) and moderate σ (10^3 S/m)3. Oxygen vacancy engineering in $CaMnO_3$ enhances σ by increasing Mn^{3+}/Mn^{4+} ratios, achieving $ZT \approx 0.37$ at 900 K26 24. The low κ (~3 W/m·K) in these materials stems from mass contrast scattering between A/B-site cations and oxygen vacancies 28.

Double Perovskite Oxides

Double perovskites like Ba_2MgWO_6 and Ca_2ZrTiO_6 enable bandgap reduction (3.17 eV → 1.87 eV) via Ni substitution, enhancing visible-light absorption and α (~400 μV/K). First-principles calculations predict $ZT \approx 4.4$ at 500 K for strained Ca_2ZrTiO_6,
52 though experimental validation is pending. The rock-salt ordering of B/B′ cations in $A_2BB'O_6$ structures further reduces κ by introducing phonon-scattering interfaces 29.

Strategies for Enhancing Thermoelectric Performance

Doping and Defect Engineering

- **n-Type Doping**: Substituting Sn^{2+} with Sb^{3+} in $CsSnI_3$ increases σ to 10^2 S/cm while maintaining $\alpha > 200$ μV/K30.
- **p-Type Doping**: La^{3+} doping in $SrTiO_3$ introduces hole carriers, boosting σ by 3 orders of magnitude28.
- **Halogen Substitution**: Cl^- doping in $CsSnI_3$ forms a surface charge reservoir, enhancing σ without degrading bulk mobility30.

Nano structuring and Composite Design

Reducing grain boundaries in 2D Ruddlesden-Popper perovskites (e.g., $(BA)_2MA_{n-1}Pb_nI_{3n+1}$) suppresses bipolar thermal conduction, lowering κ to 0.5 W/m·K 28. Embedding single-atom catalysts (e.g., Pt, Au) into perovskite matrices enhances interfacial charge transfer, improving $\alpha^2\sigma$ by 40% 35.

Challenges with perovskite

Environmental Stability

The Relentless Assault of the Environment

Like a fragile blossom thriving only in a greenhouse, perovskite materials wilt swiftly when exposed to the elements. Their most glaring vulnerability lies in their sensitivity to environmental factors, a limitation that haunts every application domainfrom solar cells to thermoelectric In high humidity (above 80% relative humidity), water molecules infiltrate the lattice, triggering hydration pathways that reduce operational lifetimes from thousands of hours to just a few [36]. Sunlight, once the perovskite's ally in photovoltaic conversion, turns foe under oxygen-rich conditions, generating superoxide radicals that catalyze crystal decomposition [38,]. Add ultraviolet light to this cocktail, and degradation accelerates dramatically, with lifespans plummeting from over 8,000 hours in dry air to a mere 10 hours under combined UV and moisture stress [39].This profound environmental fragility necessitates advanced encapsulation strategies and currently restricts deployment in unregulated or outdoor conditions [40 ,41].

2. The Toxic Legacy of Lead

Beneath the promise of perovskite technology lurks a quiet menace: lead. The very element that enables high optoelectronic performance in many halide perovskites also poses an outsized threat to ecosystems and human health. Unlike traditional lead pollutants, perovskite-derived lead is highly bioavailable, entering plant systems and, by extension, the food chain at rates up to ten times higher than other sources [42]. Its water-soluble halide forms are mobile, infiltrating soil and water systems with ease,

raising alarms among environmental regulators [40, 44]. Given this enhanced mobility and uptake, there's growing consensus that perovskite-based devices may require stricter oversight than conventional lead-containing electronics [42 40 44].

3. Scaling the Summit of Manufacturing

Translating perovskite breakthroughs from the lab bench to the production line is no trivial feat. Laboratory prototypes boast dazzling efficienciesup to 26.1%but these numbers tend to dull when scaled to industrial-sized modules, often dropping to around 22.7% [42]. The culprit? Non-uniform film deposition, increased dead zones, and the need for highly controlled atmospheres during fabrication [40]. Despite improvements, the **levelized cost of electricity (LCOE)** for perovskites still lags behind more established players like silicon and cadmium telluride, complicating commercial viability [40]

Application-Specific Fault Lines

In **solar applications**, the promise of perovskites is tempered by internal chaos. Ion migrationa silent saboteurinduces current-voltage hysteresis and performance instability over time [44]. Heat becomes an enemy as well: classic methylammonium lead iodide ($MAPbI_3$) undergoes structural changes at a modest 54°C, undermining long term performance Complicating matters further are interfacial challenges: recombination losses at charge transport boundaries and buried interfaces resist optimization due to their inaccessibility [44, 48]. Contact degradation, especially at electrode junctions, further chips away at efficiency and stability .

In thermoelectric applications, the gap between aspiration and achievement yawns even wider. While perovskites offer naturally low thermal conductivitya desirable traittheir figure of merit (ZT) remains woefully low, with leading values hovering around 0.14far short of the 1.0 benchmark needed for real-world deployment [50, 51]. Poor electrical transport properties and suboptimal doping restrict carrier mobility and power factors. Even where phonon scattering is minimized, contact resistance and poor interface design negate the advantages, severely limiting energy conversion efficiency in thermoelectric generators [24].

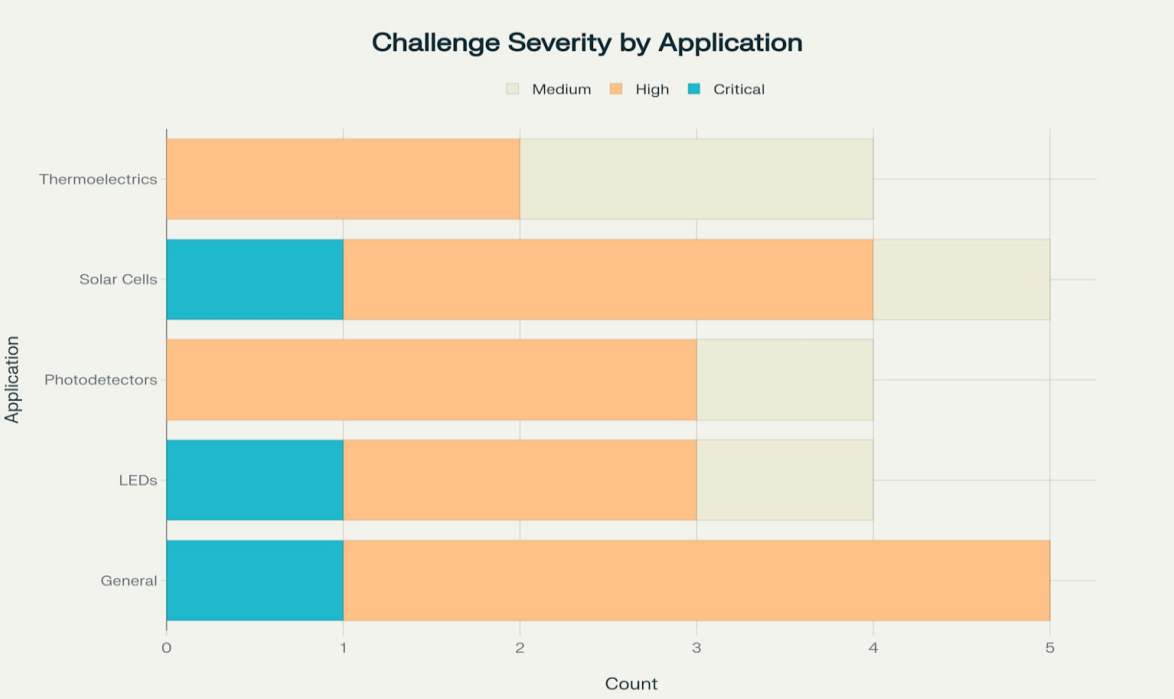


Fig. 1: *Severity of Challenges Faced in Various Perovskite Applications*

Light-Emitting Diodes (LEDs)

The Blue Dilemma In the spectrum of innovation, blue perovskite LEDs remain a tantalizing but elusive achievement. Despite promising strides, their external quantum efficiency (EQE) stubbornly lingers at around 5%, far below the desired benchmark of 20% [53,28]. This performance gap is not merely a matter of device engineering; it reflects a deeper material conflictwhere the bandgap tuning necessary for stable blue emission inherently disrupts the structural integrity of the perovskite itself [53]. Color instability and wavelength drift plague long-term operation, undermining the reliability essential for commercial viability. While green and red perovskite LEDs exhibit higher efficiency and slightly improved operational stability, they, too, fall short when compared to conventional LED technologies [28].

Photodetectors: The Mirage of Sensitivity

Perovskite-based photodetectorstouted for their high detectivity and spectral responsivenessface their own unique bottlenecks. Chief among them is a lack of measurement standardization, which often results in inflated detectivity claims due to flawed photogain calculations and underappreciated noise sources [55, 56].

Moreover, high-gain devices frequently trade off fast response times, with some registering delays of several secondsan unacceptable latency for real-time applications [55, 56]. As with other optoelectronic devices, interface instability and environmental degradation further erode performance over time, emphasizing the need for robust protective strategies [55].

Strategies for Resilience: Better Perovskite Future

1. Environmental Shielding and Structural Reinforcement

To battle environmental fragility, researchers are exploring a multi-pronged approach. Encapsulation techniques have evolved rapidly, offering improved resistance against moisture, oxygen, and UV light . Meanwhile, 2D/3D hybrid structures and mixed-cation compositions provide enhanced thermal and phase stability by reducing lattice strain and suppressing unwanted phase transitions [57].

2. Detoxifying the Chemistry

In response to growing concerns over lead toxicity, efforts are underway to develop tin-based perovskites as safer alternatives. Though these materials currently underperform and degrade faster in ambient air, their potential as low-toxicity solutions remains compelling [58].

3. Interface Engineering

The complex dance of charge carriers at material boundaries demands meticulous interface design. Passivation strategies, including self-assembled monolayers and interlayer modifications, are being employed to reduce recombination losses and bolster device lifetimes [39].

4. Compositional Design and Doping

To address structural and thermal instabilities, scientists are experimenting with compositional engineeringspecifically, mixing halide anions and A-site cations to tailor bandgaps and suppress degradation [60]. These efforts also help minimize hysteresis and phase segregation under operational stress.

5. Scalability and Cost Efficiency

Despite impressive laboratory demonstrations, the road to commercial-scale production remains bumpy. Innovations in film deposition techniques, such as blade coating and vapor-assisted methods, are helping bridge the performance gap between small-area cells and full-scale modules . Cost-reduction strategies now emphasize earth-abundant materials, simplified fabrication steps, and process standardization to make perovskite technologies economically competitive [61].

Introduction to Halide Perovskites

Few materials have transformed modern materials science as profoundly as halide perovskites. Defined by the versatile ABX_3 crystal structure, where *A* is a monovalent cation (e.g., MA^+, FA^+, Cs^+), *B* is a divalent metal (commonly Pb^{2+} or Sn^{2+}), and *X* is a halide ion (I^-, Br^-, or Cl^-), this structure offers an unparalleled platform for property tuning [62].

Architectural Variants

At the heart of the halide perovskite structure lies a three-dimensional framework of corner-sharing BX_6 octahedra, enclosing A-site cations in cuboctahedral cavities . Structural variations arise through intentional modifications at the A and B sites, leading to distinct forms with unique functionalities:

1. 3D Perovskites: The classic ABX_3 framework with continuous octahedral connectivityideal for solar cells and LEDs [39].

2. 2D Layered Perovskites: Large organic A-site cations create quantum well-like structures, increasing environmental resilience and confinement effects [64].
3. Double Perovskites ($A_2BB'X_6$): These offer lead-free alternatives with promising optoelectronic properties, substituting toxic Pb with combinations like Bi^{3+} and Ag^{+} or Sb^{3+} and Na^{+} [–].

Problem and benefits

Benefits and Advancements in Halide Perovskites

A key limitation in halide perovskites is their intrinsic halide mobility, which can lead to complete halide exchange upon exposure to an excess of different halide ions. This behavior can significantly affect device stability and operational reliability . Mixed-halide systems are particularly vulnerable, as they undergo light-induced phase segregation, which degrades optical and electronic performance .

Lead-Free Halide Perovskites: Toward Safer Alternatives

In response to environmental and health concerns regarding lead, multiple lead-free perovskite systems have been explored:

Tin-Based Perovskites ($ASnX_3$)

Tin-based perovskites represent the most promising replacements for lead-based analogs due to their similar band structures and favorable charge transport properties . Compounds like $MASnI_3$ and $FASnI_3$ have achieved power conversion efficiencies (PCEs) exceeding 13% . However, their commercial viability is hindered by the easy oxidation of Sn^{2+} to Sn^{4+}, leading to self-doping, increased conductivity, and a decline in photovoltaic performance over time [62].

Germanium-Based Perovskites ($AGeX_3$)

Germanium offers another route toward lead-free perovskites. Materials such as $MAGeI_3$ exhibit band gaps of 1.9–2.0 eV, making them ideal for tandem solar cells and other optoelectronic devices [66]. Notably, $LiGeCl_3$, as investigated in the current study,

demonstrates a direct band gap of 1.01 eV, a Seebeck coefficient of 243 μV/K, and a ZT value of 0.75 at 75°C, showcasing its thermoelectric potential [67].

Tin-Germanium Alloy Perovskites

Alloying tin with germanium, as in $CH_3NH_3Sn_{1-x}Ge_xI_3$, enhances material stability while retaining suitable bandgap tunability (1.3–2.0 eV) . The presence of Ge partially suppresses Sn oxidation, though long-term durability still falls short of lead-based counterparts [68].

Bismuth and Antimony-Based Perovskites

Structures such as $A_3B_2X_9$ (B = Bi, Sb) are appealing for their non-toxicity and superior stability, despite wide band gaps (>2 eV) and relatively low PCEs (<3%) due to poor charge transport and low-dimensional electronic structures [69]. These materials are well-suited for applications demanding durability over efficiency.

Double Perovskites ($A_2BB'X_6$)

Double perovskites offer both environmental compatibility and material tunability. For example, $Cs_2AgBiBr_6$ is known for excellent thermal and moisture stability and low lattice thermal conductivity (~0.21 W/m·K) [70]. Novel compounds such as A_2NaIO_6 (A = Ca, Sr) have achieved simulated ZT values of 0.724 and 0.686 at 1000 K, indicating high thermoelectric promise [71].

Thermoelectric Applications of Halide Perovskites

Low Thermal Conductivity

Halide perovskites exhibit ultralow lattice thermal conductivity (typically 0.3–0.5 W/m·K at room temperature), arising from strong phonon scattering and anharmonic

lattice vibrations . Features like dynamic disorder and rattling A-site cations further reduce heat transport, favoring thermoelectric efficiency [72].

Optimized Electronic Transport

Controlled doping, such as mild oxidation of Sn^{2+} to Sn^{4+} in $CsSnI_3$, can increase electrical conductivity while maintaining a stable Seebeck coefficient. Theoretical predictions suggest ZT values up to 1–2, though experimental results often remain <0.2 due to difficulties in dopant control and structural degradation [73].

Lead-Free Thermoelectric Materials

Beyond halides, oxide-based and hybrid lead-free perovskites also show strong thermoelectric potential. $LiGeCl_3$ exhibits thermal conductivity of 0.4 W/m·K at 800°C and electrical conductivity of $0.62 \times 10^4\ \Omega^{-1}\cdot m^{-1}$. Similarly, $CuLuO_3$, examined in this thesis, offers unique electronic features, while anti-perovskites like Sr_3BiN have predicted ZT values of 1.49 at 900 Kamong the highest reported for this material class [74].

Strategies for Enhancing Performance and Stability

Compositional Engineering

Mixed halide and cation compositions offer enhanced moisture resistance and thermal stability while tuning electronic properties . Incorporating cesium or rubidium and partially substituting iodide with bromide improves resilience against environmental stressors [75].

Interface and Surface Passivation

Surface treatments, including sulfur-oleylamine layers, significantly reduce defect densities and improve moisture stabilitywith devices retaining over 70% efficiency after two weeks at ~40% relative humidity [76].

Dimensionality Engineering

2D and quasi-2D perovskites integrate hydrophobic organic spacers that act as natural barriers to moisture and oxygen . These structures enhance environmental stability and enable bandgap tuning, though they often suffer from limited out-of-plane charge mobility [77].

Advanced Encapsulation

Encapsulation is essential not only for protecting device components but also for containing toxic halide ions, which pose risks to ecosystems (e.g., iodide toxicity to plants at 50 μM) . Effective encapsulation ensures long-term device reliability and environmental safety [78].

CHAPTER 2

INVESTIGATED MATERIAL AND COMPUTAIONAL RESULTS

LiGeCl3

Study from reference paper

In the relentless pursuit of sustainable, high-performance energy materials, the world of halide perovskites continues to reveal hidden gemssome already synthesized, others still locked within the equations of theoretical physics. Among the latter lies **$LiGeCl_3$**, a compound not yet seen in the laboratory, but vividly imagined through the lens of **first-principles quantum calculations**.

A product of density functional theory (DFT)-driven exploration, **$LiGeCl_3$** belongs to the **$LiGeX_3$ (X = Cl, Br, I)** family, where each halide variant offers its own electronic subtleties. the chloride compound, with its compact ionic radii, that has drawn particular attention from theorists. The compound crystallizes in the **cubic perovskite lattice** (space group **Pm-3m**), a well-known architecture celebrated for its tunable electronic landscape and structural simplicity.

Within this lattice:

- **Lithium ions** occupy the **corner sites** (Wyckoff position 1a),
- **Germanium** resides at the **center of the cube** (1b),
- while **chlorine atoms** settle into the **face centers** (3c), embracing the Ge atom in an octahedral coordination.

The chloride compound, noted for its compact ionic radii, crystallizes in a cubic perovskite lattice (space group Pm-3m). Its structural simplicity and tunable electronic landscape continue to captivate theorists.

Why $LiGeCl_3$ Deserves Attention

1. $LiGeCl_3$ stands apart in the perovskite family for several compelling reasons. First, it boasts a **toxicity-free composition**. Unlike lead-based alternatives like $MAPbI_3$ or $FAPbBr_3$, $LiGeCl_3$ is inherently lead-free, aligning perfectly with the modern demand for environmentally friendly materials in energy technologies.

Optoelectronic Promise

DFT simulations confirm that $LiGeCl_3$ has a direct bandgap with values of:

- 0.729 eV (PBE-GGA)
- 0.865 eV (GW)
- 0.965 eV (HSE06)

Shifting these toward the 1.1–1.8 eV range—the optimal window for light harvesting—positions $LiGeCl_3$ as a promising candidate for solar cell integration and potentially thermoelectric conversion.

Favorable Thermoelectric Traits

The Goldschmidt tolerance factor (t) indicates structural harmony in perovskites.

For $LiGeCl_3$, the calculated t is 0.73.

Although slightly below the ideal range (0.8 to 1.11), this suggests a distorted but stable perovskite structure (possibly non-cubic).

Similar trends in halide compounds indicate $LiGeCl_3$ may exhibit favorable structural characteristics with potential thermoelectric properties.

Table 1: *Tolerance Factor of LiAX3*

Tolerance factor of $LiAX_3$.

Species	Tolerance Factor	
	Computed	Reported [100]
$LiGeF_3$	0.73	0.66
$LiGeCl_3$	0.72	0.67
$LiGeBr_3$	0.72	0.67
$LiGeI_3$	0.72	0.67
$LiSnF_3$	0.67	0.60
$LiSnCl_3$	0.68	0.62
$LiSnBr_3$	0.68	0.62
$LiSnI_3$	0.68	0.63

Computational Blueprint and Findings

The detailed characterization of $LiGeCl_3$ was achieved through a suite of advanced DFT techniques:

- **PBE-GGA** functionals captured the structural and elastic behavior,
- **HSE06** hybrid functionals refined electronic band structure predictions,
- and the **GW approximation** provided a higher-fidelity account of quasiparticle interactions.

Additional simulations involved **supercell expansions (2×2×2)** to model real-world lattice interactions, revealing structural coherence over longer ranges and confirming the absence of unstable vibrational modeskey indicators of potential experimental viability.

The compound's **mechanical robustness**, evidenced by calculated elastic constants, and **optical responsiveness**, including a broad absorption spectrum and high optical conductivity, complete its profile as a highly multifunctional energy material.

As of now, **$LiGeCl_3$ remains a theoretical construct**, awaiting the transition from simulation to synthesis. Its journey to real-world application hinges on:

- **Controlling defects and impurities** during fabrication,
- Identifying scalable **synthesis pathways** such as **sol-gel**, **vacuum deposition**, or **hydrothermal techniques**,

- And conducting **thermal and chemical stability tests** under ambient and elevated operational conditions.

With its **lead-free composition**, **favourable energy conversion parameters**, and **tuneable functional properties**, $LiGeCl_3$ stands poised as a promising candidate for the next generation of sustainable materialsparticularly at the intersection of photovoltaics, thermoelectric, and optoelectronics.

LiGeCl3 Properties

Property	Value
STRUCTURAL PROPERTIES	
Lattice Constant (B3LYP/LanL2DZ)	5.40 Å
Lattice Constant (Literature)	5.20 Å, 5.19 Å
Unit Cell Volume	157.46 Å³
Crystal System	Cubic
Space Group	Pm-3m (221)
Li-Ge Bond Length	3.63 Å
Cl-Ge Bond Length	2.33 Å
Cl-Cl Distance	4.46 Å
Li-Cl Bond Length	2.63 Å
Li-Ge-Cl Bond Angle	46.26°
Cl-Ge-Cl Bond Angle	92.53°
ELECTRONIC PROPERTIES	
Band Gap (PBE-GGA)	0.729 eV
Band Gap (HSE06)	1.559 eV
Band Gap (GW Approximation)	1.510 eV
Band Gap (B3LYP/LanL2DZ)	1.38 eV

Table 2: *Structural and Compositional Information of $LiGeCl_3$ Perovskite*

The methodology and Results

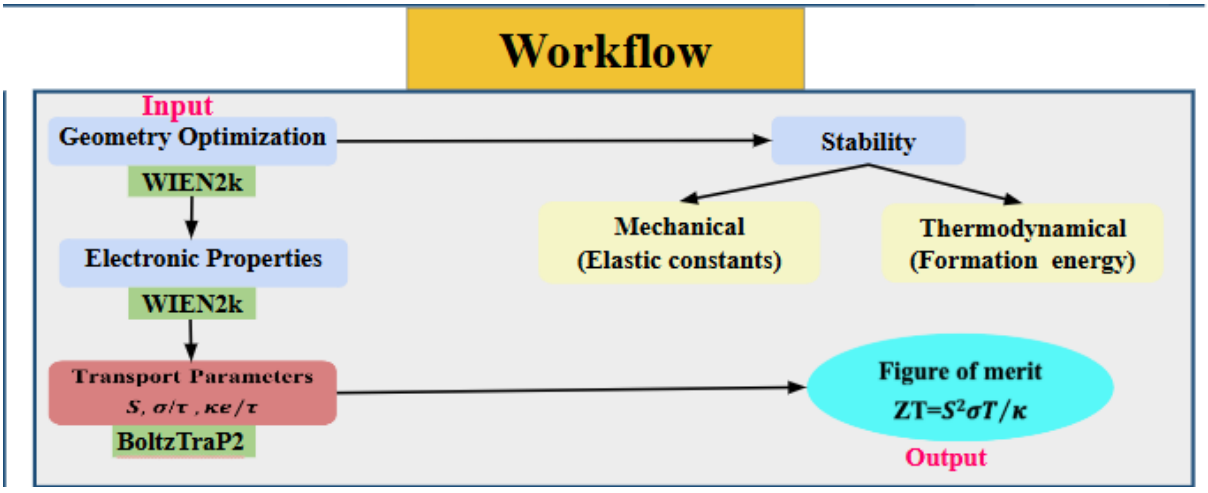


Fig. 2: *The workflow*

What we've laid out here is a hands-on, first-principles workflow to evaluate how well a material can perform as a thermoelectric—specifically, its ZT value, which tells you how efficiently it can turn heat into electricity. This isn't just about crunching numbers. It's about building a method that combines Density Functional Theory (DFT) with Boltzmann transport calculations, and making sure we don't lose sight of real-world performance—things like stability and durability.

We start with structural optimization using WIEN2k, which runs on the FP-LAPW method. This step is all about getting the geometry right—minimizing the total energy by fine-tuning atomic positions, lattice constants, and volume. Without this, nothing else that follows would be trustworthy. The way atoms are arranged has a huge influence on how the material behaves electronically.

Once the structure is settled, we move on to electronic structure calculations. This still happens within the DFT framework, again using WIEN2k. From here, we get data like the band structure, density of states (total and orbital-specific), band gap, and Fermi level. These are not just numbers—they are indicators of how charge carriers move and how much resistance or advantage the material offers for thermoelectric behavior.

The electronic data then feeds into BoltzTraP2, which uses semi-classical Boltzmann transport theory under the Constant Relaxation Time Approximation. This gives us key transport metrics:

- The **Seebeck coefficient (S)**, which tells us how much voltage you get from a temperature difference.
- The **electrical conductivity (σ/τ)**, tied to how easily carriers move.

- The **electronic thermal conductivity (κ_e/τ)**, showing how much heat is carried by the electrons.
- And the **power factor ($S^2\sigma$)**, which is a solid marker for thermoelectric efficiency.

28 But to get the full ZT value, we also need the total thermal conductivity (κ), which includes both the electronic part (κ_e) and the lattice part (κ_l). κ_e comes straight from the BoltzTraP2 output. For κ_l, though, we either turn to earlier research or run additional simulations—like using Density Functional Perturbation Theory (DFPT) or molecular dynamics—to fill that gap. It's an important piece, even if it's not part of the main workflow chart.

Finally, none of this matters if the material falls apart in real life. So, stability checks are built into the process to make sure we're not just finding good numbers, but materials that can actually be made and will hold up under operating conditions. That's the only way any of this becomes useful beyond the screen.

1. Mechanical Stability

Mechanical robustness is examined via the **elastic constants (C_{ij})**, computed using **DFT**. These constants are benchmarked against the **Born–Huang mechanical stability criteria**, which vary depending on the crystal system. For instance, in a **cubic lattice**, the following inequalities must hold:

$C_{11} > 0$

$C_{44} > 0$

$C_{11} - C_{12} > 0$

Satisfying these conditions confirms that the crystal can withstand small deformations without structural failure.

2. Thermodynamic Stability

The **formation energy (E_{xrm})** is computed to assess the material's thermodynamic favorability. It is calculated as:

$$E_f = E_{compound} - \sum_i n_i \mu_i$$

where:

- Ecompound is the total DFT energy per formula unit of the material,

- n_i is the number of atoms of element iii,
- μ_i is the chemical potential of element iii in its standard reference state (typically the elemental solid or gas).

A **negative formation energy** indicates that the material is thermodynamically stable and resistant to spontaneous decomposition into its elemental constituents.

Final Evaluation: Thermoelectric Figure of Merit

The culmination of this multistep computational approach is the evaluation of the dimensionless **figure of merit (ZT)**, given by:

$$ZT = \frac{S^2 \sigma T}{\kappa}$$

where:

- S is the **Seebeck coefficient**,
- σ is the **electrical conductivity**,
- T is the **absolute temperature**, and
- $\kappa = \kappa e + \kappa l$ is the **total thermal conductivity**.

A higher ZT value means the material is better at thermoelectric performance—it can turn heat differences into electrical power more efficiently while keeping thermal losses low.

This kind of first-principles computational approach has now become a key part of materials informatics and large-scale screening for new thermoelectric materials. Since it offers reliable predictions before any lab work is done, it helps speed up the entire process of discovering and developing future energy-harvesting technologies.

Structure analysis

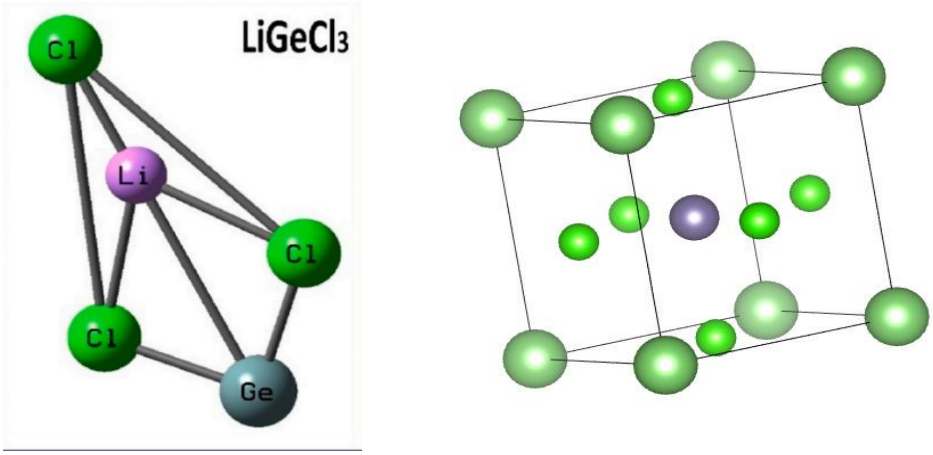


Fig.3 : *Structure of $LiGeCl_3$*

To investigate the crystal structure of $LiGeCl_3$, a first-principles approach grounded in Density Functional Theory (DFT) is utilized. Structural optimization is conducted using In the depths of scientific inquiry, the WIEN2k computational suite employs the full-potential linearized augmented plane wave (FP-LAPW) techniquea method renowned for its exceptional precision in forecasting the structural attributes of materials. This approach stands out by delving deeply into the intricacies of all-electron interactions within periodic solids, thus bypassing the need for pseudopotentials and achieving an accuracy that borders on artistry.

Crystal Structure

The journey commences with the birth of the initial crystal configuration. When fortune favors the researcher with experimental crystallographic insights often stored as CIF files in esteemed databases like ICSD or the Materials Project these records are seamlessly woven into the computational tapestry. However, when the empirical data remains elusive, it becomes imperative to craft the foundational blueprint manually, defining the unit cell parameters, atomic coordinates, and space-group symmetry with meticulous care via the StructGen module housed within WIEN2k. For substances such as $LiGeCl_3$ whose crystal habit may oscillate between orthorhombic and trigonal forms, contingent When it comes to figuring out the right structural phase, it's not just ticking a boxit's a decision that carries weight, what's already into scientific research. It's one of those moments where choosing right feels more like instinct shaped by experience than cold calculation.

There's a kind of story unfolding here, where careful theoretical work runs alongside the trial error of the lab, each step shaped by both logic and a bit of educated guesswork. It's in that mix of precision that the true spirit of modern crystallography lives.

Computational Parameters

Appropriate computing parameters for the FP-LAPW method are chosen after the structure initialization. The Generalized Gradient Approximation (GGA) in the Perdew-Burke-Ernzerhof (PBE) formulation is used for geometry optimization because it provides a good balance between accuracy and computational cost for structural calculations.

The RK_{max} parameter, which is the product of the largest plane-wave vector (K_{max}) and the smallest muffin-tin radius (R_{MT}), is an important parameter in LAPW-based computations. In order to guarantee dependable convergence, this value is typically selected between 7.0 and 9.0. To minimize the size of the basis set, the muffin-tin radii (RMTs) for the atoms Li, Ge, and Cl are chosen to be as large as feasible without resulting in overlap.

.

A Γ-centered Monkhorst-Pack k-point mesh is utilized for sure effective Brillouin Zone sampling. For systems of moderate complexity, correct total energy values are usually obtained using a grid of 10 × 10 × 10. Additionally, to ensure precise treatment of electrons during the self-consistent field process, an energy cutoff is set to set between core and valence states, typically at −6 Ry.

Structural Optimization

Structural optimization is carried out using SCF cycles run through the run_lapw script, with the right convergence options enabled. In this step, both the lattice parameters and the positions of atoms inside the cell are tweaked to bring down the total energy and atomic forces. The process is considered converged when two conditions are met:

• The total energy change is less than 0.0001 Ry per unit cell, and
• The forces on atoms drop below 1 mRy/Bohr.

The optimization can be conducted using run_lapw -fc 1.0 for force-based relaxation or with the min_lapw script, which integrates volume and shape optimization with atomic position relaxation. This iterative procedure continues until the forces on all atoms fall below the specified threshold and energy convergence is attained.

Post-Optimization Verification

So, once everything finally convergeswhich can take a bit depending on the system you'll get output files like .struct and .scf. These hold the relaxed lattice parameters and where the atoms have settled in. Now, don't just take these results at face value. You'll want to give them a proper once-overmake sure they actually make sense physically and aren't doing anything weird structurally.

The .struct file, in particular, is the one carrying the final crystallographic setup. You can throw it into something like VESTA to get a visual feel for it. That's where you check if the symmetry stayed intact, and whether the local bonding still looks reasonablenot just numbers on paper, but something that holds up in the real, atomic world.

Additionally, tracking the total energy and force evolution throughout the optimization helps confirm the smoothness and reliability of the convergence. A successfully optimized structure is considered to represent the system's ground-state configuration and can be used for further investigations such as electronic, vibrational, or thermoelectric property analyses.

Equation of State (EOS) Fitting via Murnaghan Equation

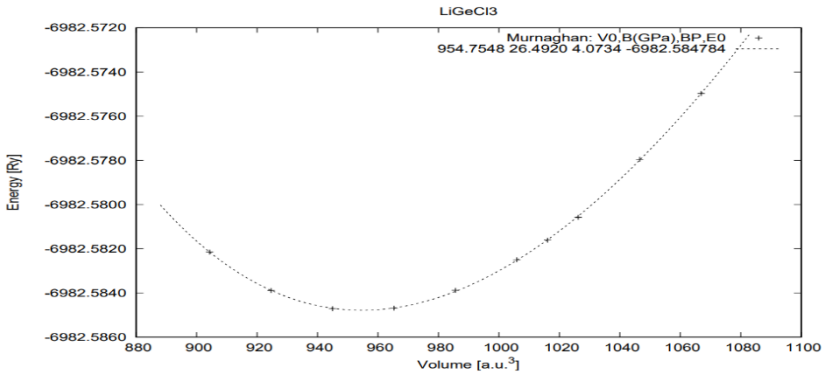


Fig.4 : *Energy vs Volume Curve for $LiGeCl_3$ Using Murnaghan Equation of State*

In this a volume optimization (or equation of state calculation) was performed to determine the equilibrium lattice volume, bulk modulus

- X-axis (Volume [a.u.³]): This represents different volumes of the unit cell, each corresponding to a separate DFT calculation where total energy is computed after fixing volume and relaxing internal coordinates.
- Y-axis (Energy [Ry]): This is the total energy of the system for each of the corresponding volumes. It's in Rydbergs (Ry), the unit used by WIEN2k.
- The Curve: The total energy values are fitted to the Murnaghan equation of state, which gives the equilibrium structural parameters by finding the minimum on this curve

Third-order Birch-Murnaghan equation of state

$$E(V) = E_0 + \frac{B_0 V}{B_0'(B_0'-1)}\left[\left(\frac{V_0}{V}\right)^{B_0'-1} + (B_0' - 1)\right] - \frac{B_0 V_0}{B_0'-1} \quad (2)$$

- E(V): Energy at volume VVV
- E0: Minimum energy (at equilibrium volume V0V_0V0)
- V0: Equilibrium volume
- B0: Bulk modulus at equilibrium
- B0′: Pressure derivative of the bulk modulus

This formula is widely used to extract bulk modulus (B_0), its pressure derivative (B_0'), and equilibrium volume (V_0) by fitting total energies computed for different volumes.

DFT Total Energy Calculations

For each deformed volume, a self-consistent field (SCF) calculation is carried out using the full-potential linearized augmented plane wave (FP-LAPW) method

implemented in WIEN2k. The exchange-correlation functional used during this step is the generalized gradient approximation (GGA) in the Perdew–Burke–Ernzerhof (PBE) formulation.
Each SCF calculation involves solving the

Kohn–Sham equations:

$$\left[-\frac{1}{2}\nabla^2 + V_{\text{eff}}(\mathbf{r})\right]\psi_i(\mathbf{r}) = \varepsilon_i\psi_i(\mathbf{r})$$

where Veff(r) includes the external, Hartree, and exchange-correlation potentials. The plane-wave basis set is determined by the RKmax parameter and the muffin-tin radii (RMT) are chosen to avoid overlapping spheres.

All internal atomic positions may also be relaxed (if desired) for each volume, or fixed to focus purely on volume dependence of total energy. The SCF calculations yield the total energy E(V) at each volume point.

Initial Structure Preparation

The process begins with defining the crystal structure of the materialin this case, **$LiGeCl_3$**. A .struct file is created that includes:

- The crystal system and lattice type (e.g., cubic, orthorhombic).
- Lattice parameters (a, b, c, α, β, γ).
- Atomic positions expressed in fractional coordinates.
- Atomic species and their muffin-tin radii.

After the structural file is prepared, an initialization procedure is carried out. This includes specifying the plane-wave cutoff (RKmax), generating the k-point mesh for Brillouin zone sampling, defining atomic sphere radii, and initializing the electronic potential.

Volume Scaling

To construct the E–V curve, total energy calculations are performed at various scaled volumes around the equilibrium structure. This typically involves

generating 8 to 12 structures by uniformly scaling the unit cell volume in small increments (e.g., ±2%, ±4%, ±6%).

Each new structure corresponds to a modified volumeeither expanded or compressed relative to the initial guess. These scaled structures are created systematically, ensuring isotropic scaling so that the crystal symmetry is preserved.

Energy Calculations at Each Volume

Each of the scaled structures undergoes a **self-consistent field (SCF)** calculation To calculate the total electronic energy, the structure is evaluated at different volumes, while keeping all other computational settings like RKmax, energy convergence thresholds, and k-point mesh unchanged. This way, any change in energy directly reflects the effect of volume, not numerical noise. For each volume, an SCF calculation is carried out, and the total energy is noted. These energy-volume pairs are then collected into a dataset that can be used for fitting an equation of state (EOS).

Fitting to an Equation of State

The energy vs. volume data is fitted to an analytical **equation of state** to extract equilibrium parameters. WIEN2k supports multiple fitting models, the most common being the **Murnaghan equation of state**. Other supported models include Birch–Murnaghan and Vinet EOS.

The fitting yields key physical parameters:

- **Equilibrium volume (V_0)**: The volume at which the total energy is minimized.
- **Bulk modulus (B_0)**: Quantifies the material's resistance to uniform compression, typically expressed in GPa.
- **Pressure derivative of bulk modulus (B'_0)**: Describes how the bulk modulus changes under applied pressure.
- **Minimum total energy (E_0)**: The ground-state energy corresponding to the equilibrium configuration.

The result is usually visualized as a smooth, parabolic E–V curve with a distinct minimum.

Interpretation and Use

The **minimum of the E–V curve** indicates the structure's most stable configuration under zero pressure. This **equilibrium volume** is used in subsequent calculations to ensure accurate and physically meaningful results. It forms the basis for further evaluation of:

- **Electronic structure** (band structure, density of states).
- **Transport properties** (via BoltzTraP or similar tools).
- **Phonon spectra** and **vibrational analysis**, if coupled with lattice dynamics codes.
- **Mechanical stability** via calculation of elastic constants.

The **bulk modulus** and its pressure derivative give insights into the **material's compressibility and mechanical stiffness**. When the bulk modulus (B_o) is high, it points to a stiffer, more rigid structure; a lower value means the material is softer. This kind of information matters a lot for thermoelectric materials, where both mechanical strength and thermal stability play a key role in whether the material can actually be used in real conditions.

.

Density of states calculation

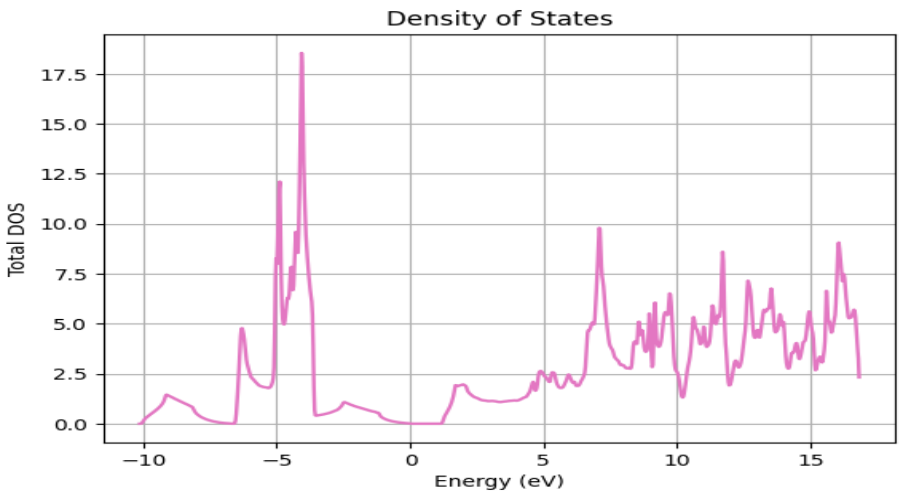


Fig. 5: *The density of state of $LiGeCl_3$*

Self-Consistent Field

It all kinda kicks off with solving the Kohn-Sham equations yeah, the ones from DFT. The goal here is to get the system to settle down into its lowest energy state. You run this loop where the electronic structure updates over and over until the charge density stops changing beyond a tiny threshold. That's when you know things have clicked into place.

This whole SCF step leans heavily on whatever exchange-correlation flavor you've picked GGA's a popular goto and it factors in both the core electrons (the quiet types) and the valence ones doing all the action. Getting solid convergence here is crucial, no shortcuts really, since the potential and charge density you get now become the bedrock for everything else that follows like density of states, band structure, all that good stuff.

Eigenvalue and Partial Charge

38 Once the self-consistent field (SCF) cycle is complete, the next step is to calculate the energy eigenvalues and partial charges. This is done using the LAPW2 module in WIEN2k, which takes the wavefunctions and projects them onto atomic-like orbitals inside the muffin-tin regions. At this point, you can also pull out the partial density of states (PDOS) by seeing how much each orbital (s, p, d, etc.) contributes. This orbital-wise breakdown is helpful when you want to look into things like chemical bonding and how orbitals mix or hybridize.

Doing more DOS Calculation

To get a good handle on the density of states, WIEN2k uses the tetrahedron method for Brillouin zone integration. What it does is slice up the reciprocal space into lots of tiny tetrahedra and then interpolate the energy inside each one. When you add everything together from all those little shapes, you end up with a DOS that's not just smooth, but actually pretty accurate.

This method really shines when it comes to picking up sharp features in the electronic structure things like van Hove singularities that would probably get lost if you were

just using something simpler like Gaussian smearing. It's especially useful for materials with complicated band structures, where those fine details matter.

Once this step wraps up, WIEN2k gives you files with the total and partial density of states. If spin polarization is part of the setup, you'll see separate data for spin-up and spin-down. The total DOS shows the full spread of electronic states across the system, while the PDOS breaks it down further, so you can tell which atoms or orbitals are contributing to what.

Customization of Energy Range and Resolution

The energy window over which the DOS is calculated, along with the number of points sampled, can be customized by modifying the input parameters. This is particularly useful for focusing on regions near the Fermi level, such as the valence band maximum or conduction band minimum, which are most relevant for semiconducting or thermoelectric behavior. A higher number of sampling points results in a smoother DOS curve with better resolution of fine spectral features.

Visualization and Interpretation

Although WIEN2k does not include a built-in graphical interface for plotting DOS, the numerical output can be readily visualized using external plotting software. The resulting graph typically presents energy on the x-axis and DOS on the y-axis, with the Fermi energy aligned at zero. Peaks in the DOS indicate high densities of available states, which may correspond to flat bands or localized states in the band structure. A band gap is identified as a region of zero DOS near the Fermi level, characteristic of semiconductors or insulators, while a non-zero DOS at the Fermi level signifies metallic behavior.

In materials like thermoelectric compounds, what the density of states (DOS) looks like around the Fermi level tells you a lot about how carriers behave and how easily they move. If there's a sharp peak or feature close to the Fermi level, it can actually boost the Seebeck coefficient. This happens because such features create more imbalance in how electronic states are distributed with respect to energy, which helps with thermoelectric performance.

Electronic Structure Analysis

Electronic Structure Analysis Methodology

We explored the electronic structure of the material using first-principles density functional theory (DFT). The idea was to closely examine things like the band gap and how electrons behave across energy levels. For this, we worked with the WIEN2k simulation package, which is based on the full-potential linearized augmented plane wave (FP-LAPW) method. This method doesn't cut corners it treats both core and valence electrons equally and doesn't make any simplifying assumptions about the potential or charge density. So, in terms of DFT methods, this is among the most reliable when it comes to getting accurate results, whether you're looking at structure or electronic behavior.

We began by doing a complete structural optimization using the Perdew-Burke-Ernzerhof (PBE) form of the exchange-correlation functional. In this approach, the exchange-correlation energy is handled using the Generalized Gradient Approximation (GGA), which offers a good balance between accuracy and computational efficiency.

Because of its balanced accuracy and computational efficiency, GGA-PBE is frequently used to estimate atomic locations, bond lengths, and equilibrium lattice constants. 10 x 10 × 10

Γ-centered k-mesh was used to sample the Brillouin zone (BZ), guaranteeing dense and consistent k-point coverage to capture the subtleties of the electronic states. To distinguish between core and valence states, the energy cut-off was chosen at -6 Ry. By bringing the overall energy variation down to less than 0.0001 Ry per unit cell, self-consistent convergence was guaranteed.

Electronic Band Structure and Band Gap Correction

After structural convergence, the electronic band structure was computed. As shown in the first plot, the band structure derived using the GGA functional underestimates the electronic band gap, a well-known limitation of conventional semilocal DFT approximations. To address this, a more advanced meta-GGA exchange potential, namely the modified Becke-Johnson potential (TB-mBJ), was employed. This potential is particularly effective for semiconductors and insulators, as it includes kinetic energy density contributions, allowing a better approximation to the exact exchange potential and resulting in a more accurate estimation of the band gap.

The second plot depicts the band structure computed using mBJ, showing a noticeable correction to the underestimated gap observed with GGA. The Fermi energy was set at 0 eV, and the conduction band minimum (CBM) and valence band maximum (VBM) are distinctly separated, confirming the semiconducting nature of the material and revealing the indirect/direct nature and magnitude of the band gap.

Band Structure Interpretation

From the band dispersion along high-symmetry directions in the Brillouin zone, the band structure provides detailed information about the effective masses of charge carriers, band curvature, and bandgap characteristics. The mBJ-corrected band structure confirms the presence of a finite bandgap, which is critical for evaluating the thermoelectric performance and carrier transport properties. Flat regions in the valence or conduction bands suggest localized states and high effective masses, while more dispersive bands indicate higher carrier mobility.

The comparison between GGA and mBJ results highlights the necessity of using an advanced functional when the accurate bandgap is essential, especially for predictive modeling of transport properties. Such corrections are crucial for obtaining realistic Seebeck coefficients, carrier concentrations, and thermoelectric figures of merit.

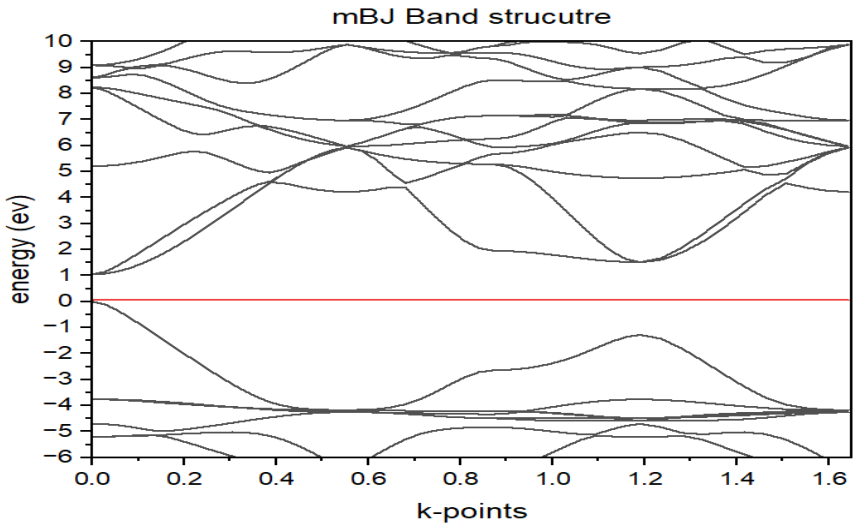


Fig. 6: *Electronic Band Structure of $LiGeCl_3$ Using mBj*

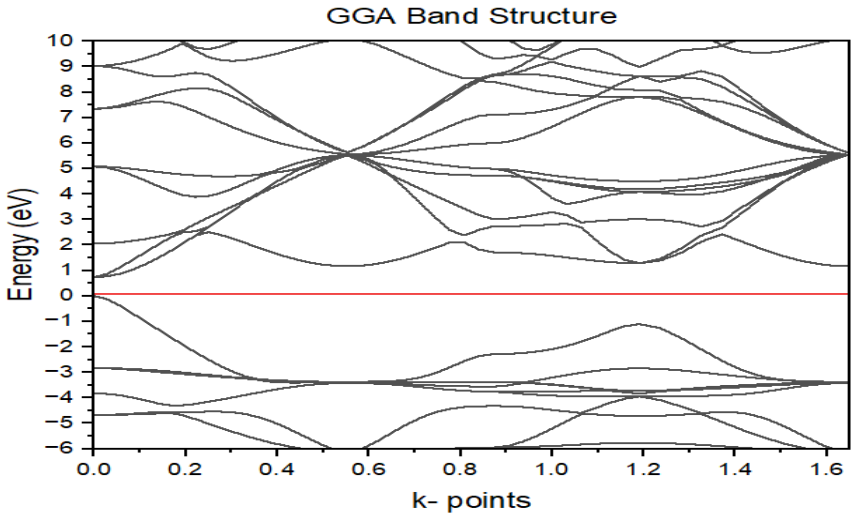


Fig. 7: *Electronic Band Structure of $LiGeCl_3$ Using GGA*

Transport Properties

To understand how transport works in the material, we started a computational journey that relied on accurate first-principles calculations and was steered by the ability of density functional theory (DFT) to work together with semiclassical transport methods. Central to our study is WIEN2k,

a great code that uses the full-potential linearized augmented plane wave(FP LAPW) approach known for it accuracy in describing the quantum movements of electrons particularly within crystals that have complexity features or contain heavy atoms.

The journey began with the careful **structural optimization** of the crystal lattice. This was performed under the watchful eye of the **Generalized Gradient Approximation (GGA)**, specifically in the Perdew-Burke-Ernzerhof (PBE) form, to handle exchange-

correlation interactions. A **Gamma-centered 10x10x10 k-point mesh** was laid over the Brillouin zone like a fine net, ensuring that no nuance of the electronic structure escaped notice. Energy convergence was demanded at a stringent **0.0001 Ry per cell**, and a **−6 Ry cut-off** was enforced to honor the boundaries between core and valence states.

Even this accuracy was not enough. The GGA, great as it is, most of the time hints smaller band gaps than what the real world hasan underestimation that sometimes clouds transport predictions. To up this veil, the Tran-Blaha modified Becke-Johnson potential was used, providing a better view for understanding the electronic structure. With its more realistic treatment of the exchange potential, TB-mBJ brought the band gap closer to reality hence adding validity to the derived properties.

Into this newly mapped landscape, we directed BoltzTraP, a code that communicates in the language of thermoelectricity. It took energy eigenvalues from WIEN2k as its base and then ran forward to solve the Boltzmann Transport Equation (BTE) in the constant relaxation time approximation (CRTA). From this, the essential transport quantitieselectrical conductivity (σ), electronic thermal conductivity (κ_e), and the Seebeck coefficient (S)were derived.

Beneath the surface, these quantities emerged from the intricate **energy-dependent conductivity tensor**, σαβ(ε), meticulously integrated over the Fermi surfacewhere electrons hover on the brink of motion, defining the behaviour of materials in the presence of heat and charge.

ELECTRICAL CONDUCTIVITY WITH TEMPERATURE

$$\sigma_{\alpha\beta}(\mu, T) = \frac{1}{\Omega}\int \sigma_{\alpha\beta}(\epsilon)\left(-\frac{\partial f}{\partial \epsilon}\right) d \quad (3)$$

- σ(μ, T): Electrical conductivity as a function of chemical potential (μ) and temperature (T).
- Ω: Represents the volume or normalization factor.
- ∫: Integral sign, indicating that conductivity is calculated over a range of energy levels.
- σ(ε): Conductivity at a specific energy level (ε).
- (-∂f/∂ε): Derivative of the Fermi distribution function, which describes how electrons occupy energy states

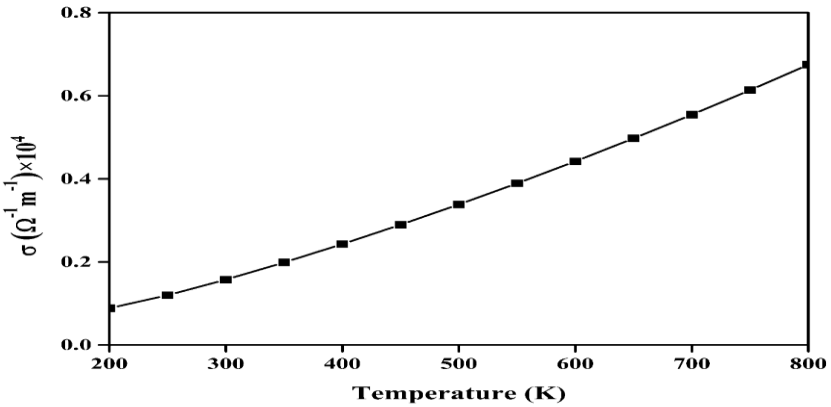


Fig. 8: *Electrical Conductivity vs. Temperature*

The graph shows that the electrical conductivity of $LiGeCl_3$ increases steadily as the temperature rises. This positive trend is typical of thermally activated conduction processes. In $LiGeCl_3$, as the material is heated, more charge carriers are likely generated or mobilized, which results in higher conductivity. The nearly linear trend in the conductivity data (when plotted appropriately) indicates that the conduction mechanism remains consistent over the temperature range studied, without a sudden transition to metallic behaviour.

THERMAL CONDUCTIVITY WITH TEMPERATURE

$$\kappa^{e}_{\alpha\beta}(\mu, T) = \frac{1}{e^2 T\Omega}\int \sigma_{\alpha\beta}(\epsilon)(\epsilon-\mu)^2\left(-\frac{\partial f}{\partial \epsilon}\right)d$$

- $\kappa^{(e)}_{(\alpha\beta)}(\mu, T)$: Represents the electronic thermal conductivity tensor as a function of the chemical potential (μ) and temperature (T).
- e^2, T, Ω: Here, e is the fundamental charge, T the temperature, and Ω is the volume (or normalization factor).
- $\int$: The integral sums contributions over energy levels (ε).
- $\sigma_{(\alpha\beta)}(\varepsilon)$: The energy-dependent electrical conductivity tensor.
- $(\varepsilon - \mu)^2$: Weighs each energy level by how far it deviates from the chemical potential, which is key for heat transport calculations.
- $-\partial f/\partial \varepsilon$: The derivative of the Fermi-Dirac distribution, representing how electron occupancy changes with energy.

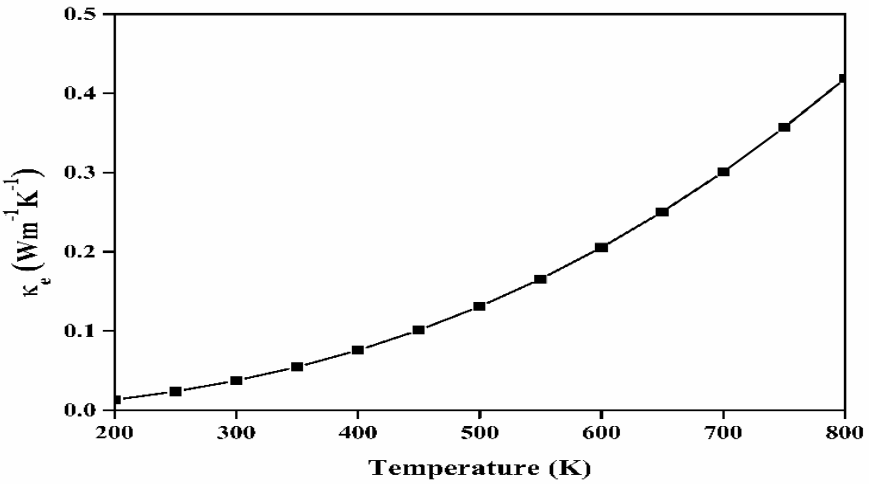


Fig. 9: *Thermal Conductivity vs. Temperature*

- The thermal conductivity of the material is increasing which is a problem, can be improved using methods which help in phonon scattering.
- On the other hand the thermal conductivity is increasing which is favourable for thermoelectric properties.

3.3 Seebeck coefficient with temperature

$$S_{\alpha\beta}(\mu,T) = \frac{1}{eT\sigma_{\alpha\beta}(\mu,T)} \int \sigma_{\alpha\beta}(\epsilon)(\epsilon-\mu)\left(-\frac{\partial f}{\partial \epsilon}\right) d \quad (4)$$

- **Sαβ (μ, T):** This represents the Seebeck coefficient, expressed as a tensor. Its value depends on the chemical potential (μ) and the temperature (T), capturing how voltage is generated in response to a temperature difference.
- **e:** The elementary charge, which is the basic unit of electric charge in physics.
- **σαβ (μ, T):** The electrical conductivity tensor evaluated at the chemical potential (μ) and temperature (T). It describes how well the material conducts electricity under those conditions.
- **σαβ (ε):** The energy-dependent electrical conductivity at a specific energy level (ε).
- **ε - μ:** The difference between the electron energy level (ε) and the chemical potential (μ). This term accounts for the energy deviation that drives the thermoelectric effect.
- **-∂f/∂ε:** Represents the negative derivative of the Fermi-Dirac distribution function with respect to energy. This derivative indicates how the occupancy of electron states changes with energy, which is crucial for calculating the thermoelectric response

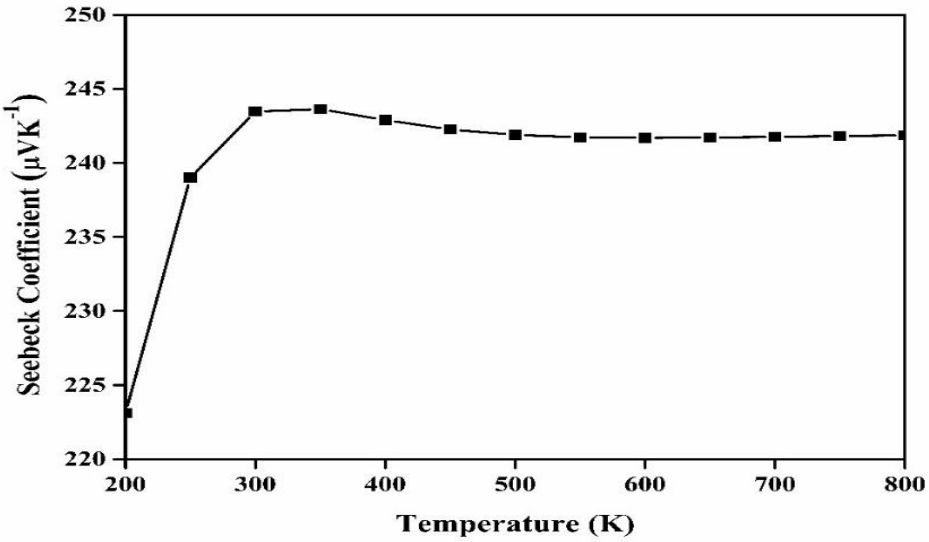


Fig. 10: *Calculated Seebeck coefficient for a range of temperature*

- The $LiGeCl_3$ have a stable seebeck effect which tells about good thermal stability about the material.
- Power factor is also increasing with temperature shows the material's thermoelectric performance improves with increasing temperature.
- The seebeck coefficient value 243μV/K at room temperature is really good as thermoelectric material.

Power factor (PF)

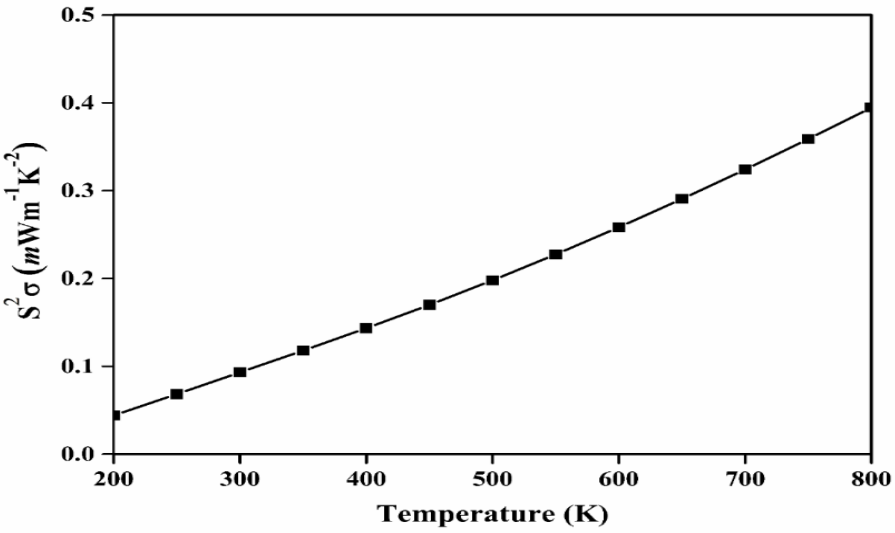


Fig. 11: *Calculated power factor for a range of temperature*

The calculated power factor exhibits a strong temperature dependence, increasing monotonically over the range of 200–800 K. This behavior is attributed to the

simultaneous enhancement of both the Seebeck coefficient and electrical conductivity at elevated temperatures. The trend is consistent with a semiconducting transport mechanism, and the high power factor at elevated temperatures underscores the potential of $LiGeCl_3$ for thermoelectric energy conversion. These results were obtained from the solution of the Boltzmann Transport Equation (BTE) using the BoltzTraP code, informed by accurate electronic structure calculations from the WIEN2k package under the TB-mBJ exchange-correlation functional.

The **power factor (PF)** is defined as:

$$PF = S^2\sigma$$

Where:

- Sis the **Seebeck coefficient** (V/K),
- σ is the **electrical conductivity** $(\Omega^{(-1)}\ m^{-1})$.

It is measured in units of $W \cdot m^{-1} \cdot K^{-2}$, and it quantifies the **electrical contribution to thermoelectric performance**. A high power factor implies the material can effectively convert heat into electrical power.

Figure of merit

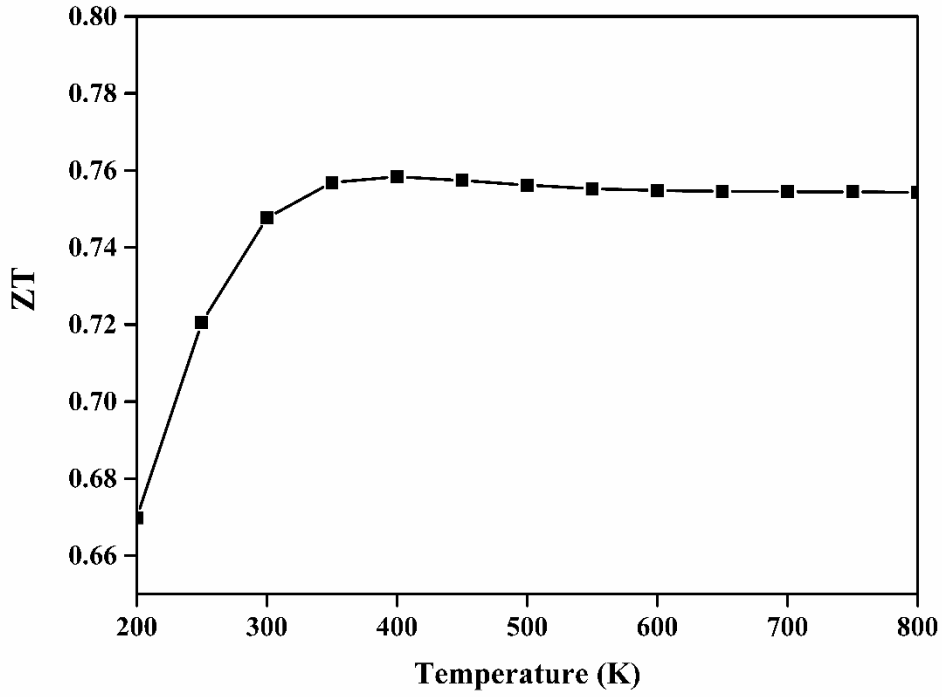


Fig. 12: *ZT against Temperature*

The result shows that $LiGeCl_3$ is a low temperature thermoelectric material with ZT value reaches to 0.75 at 75°C which remain constant throughout the range which shows performance consistency and stability of the material

- The power factor and electrical conductivity are increasing .
- The value of at 0.4 W/m·K 800°C and Electrical conductivity goes to 0.62 × 10^4 Ω.m.s at high 800°C

- The calculation of these parameters were done by solving semi classical Boltzmann transport theory and were the relaxation time is taken to be 10^{-14} seconde.

CuLuO3

$CuLuO_3$ is a novel cubic oxide-perovskite (space group Pm3m) first predicted and characterized through computational methods. There is no prior experimental or theoretical report on this compound; its properties were established using first-principles density functional theory (DFT) calculations, specifically with the CASTEP code. The study employed both the RPBE (a GGA functional) and HSE06 (a hybrid functional) to improve accuracy for electronic and optical properties. Structural stability was confirmed via formation enthalpy and phonon dispersion calculations, ensuring the reliability of the predicted phase1.

Key Parameters for Calculations

- **Crystal structure:** Cubic perovskite, space group Pm3m
- **Lattice constant:** 4.29 Å
- **Cell volume:** 79.15 $Å^3$
- **Bulk modulus:** 52.62 GPa
- **Formation enthalpy:** –10.10 keV/atom
- **Band gap:** 1.86 eV (indirect, M–Γ points)
- **Bonding:** Mixed ionic-covalent, with ionic character dominant (Mulliken analysis: Cu^0.59, Lu^1.26, O^–0.61)
-

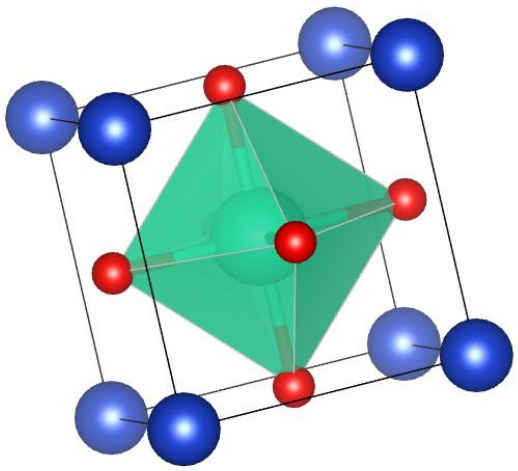


Fig. 13: *The Structure*

$CuLuO_3$ is a ternary oxide compound that crystallizes in a **perovskite-related structure** with the general formula **ABO_3**, where:

- **A = Lu^{3+} (lutetium)** – a rare-earth metal ion.
- **B = Cu^{2+} (copper)** – a transition metal.
- **O = O^{2-} (oxygen)** – forming the oxide framework.

The unit cell is **primitive cubic**, composed of:

- **8 corner atoms** (Cu), each shared among 8 adjacent unit cells ⇒ contributes **1 atom per cell**.
- **1 body-centered atom** (Lu), entirely within the unit cell ⇒ contributes **1 atom per cell**.
- **6 face-centered atoms** (O), each shared between 2 cells ⇒ contributes **3 atoms per cell**.

This leads to the correct stoichiometry of **$CuLuO_3$** per unit cell:

- 1 Cu
- 1 Lu
- 3 O

Thermal conductivity

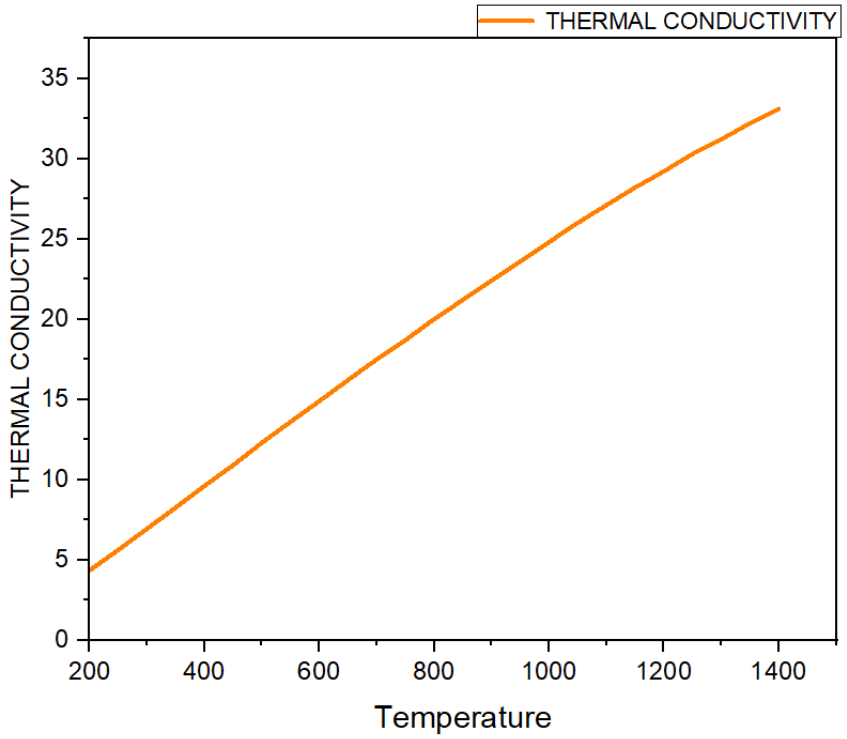


Fig. 14: *Thermal Conductivity vs. Temperature*

- **X-axis (horizontal):** Temperature (units not specified, but likely in Kelvin)
- **Y-axis (vertical):** Thermal Conductivity (units not specified, but typically W/m·K)

Key Observations:

- As temperature increases from about 200 to 1400 (presumably Kelvin), thermal conductivity rises steadily.
- The curve is smooth and upward, indicating a positive correlation between temperature and thermal conductivity for this material.
- At lower temperatures (~200 K), thermal conductivity is around 4 units.
- At higher temperatures (~1400 K), it exceeds 35 units.

The observed thermal conductivity trend in the given temperature range suggests that the material's heat transport is **strongly temperature-dependent**, likely dominated by **charge carrier contributions** rather than lattice vibrations. This must be carefully considered when evaluating the material's potential for **thermoelectric applications**, as a higher κ typically **reduces ZT** unless electrical performance is exceptional.

Electrical conductivity

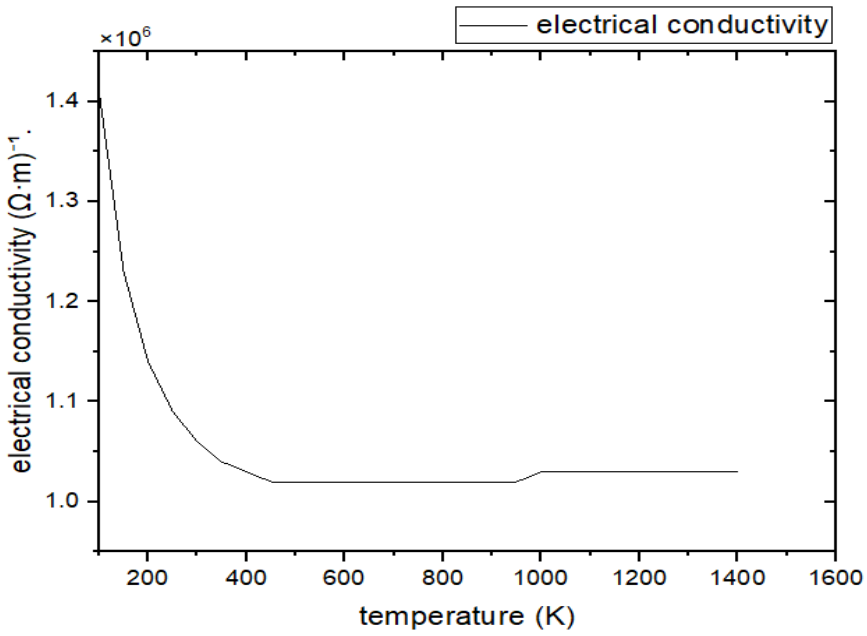


Fig. 15: *Electrical Conductivity vs. Temperature*

- **At low temperatures (below ~300 K):** Electrical conductivity starts high, around 1.4×10^6 $(\Omega \cdot m)^{-1}$.
- **As temperature increases (up to ~600 K):** Conductivity decreases sharply, reaching a minimum of about 1.0×10^6 $(\Omega \cdot m)^{-1}$.
- **At higher temperatures (above ~600 K):** The conductivity stabilizes and remains nearly constant up to 1500 K.

This behavior is typical for semiconducting materials. At low temperatures, charge carriers are less scattered, resulting in higher conductivity. As temperature rises, increased lattice vibrations (phonon scattering) reduce carrier mobility, causing conductivity to drop. Beyond a certain temperature, the number of thermally excited carriers compensates for increased scattering, resulting in a plateau in conductivity.

$CuLuO_3$ exhibits high electrical conductivity at low temperatures, a rapid decrease with increasing temperature, and then a stable conductivity at elevated temperatures. This pattern reflects its semiconducting nature and suggests stable electrical performance in high-temperature environments

The electrical conductivity behavior over a wide temperature range suggests that the material is **metallic or highly degenerate semiconducting** in nature, with limited temperature-dependent carrier activation. The flat high-T regime implies robustness in electrical performance, making the material a **promising candidate for thermoelectric or electronic high-temperature applications**, especially when coupled with appropriate thermal management strategies.

Seebeck coefficient

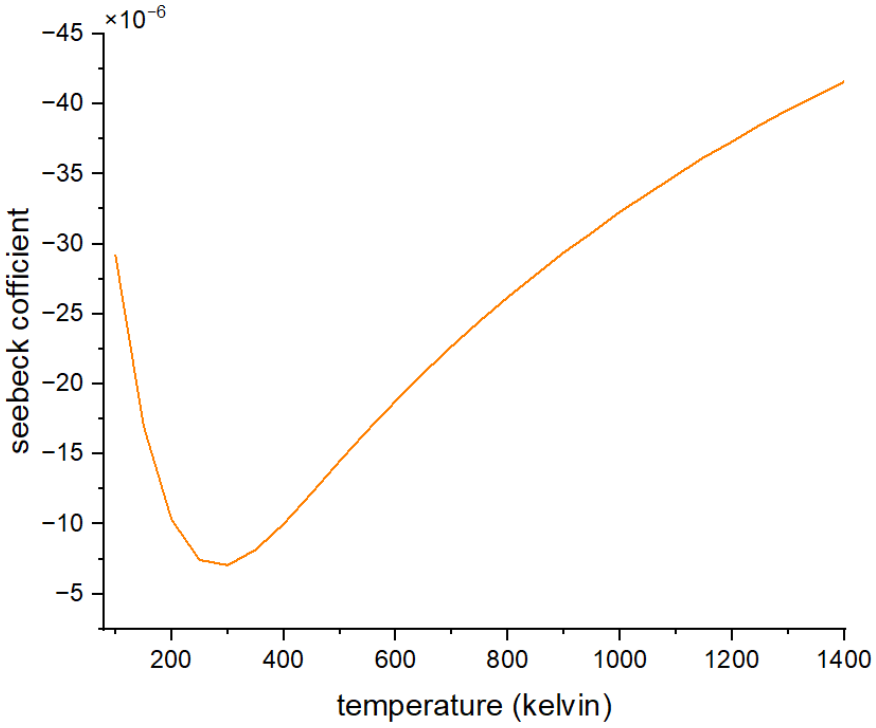


Fig. 16: *Calculated Seebeck coefficient for a range of temperature*

One of the most essential variables in assessing a material's thermoelectric performance is the Seebeck coefficient (S), which is often expressed in μV/K (or 10^{-6} V/K). It gauges how much of an induced thermoelectric voltage occurs when the material experiences a temperature gradient. The main charge carrier type is indicated by the sign of the Seebeck coefficient, which is positive for holes (p-type) and negative for electrons (n-type). The Seebeck coefficient is displayed from 200 K to 1400 K as a function of temperature in the above graph. The constant negative readings validate n-type conductivity by showing that electrons are the predominant carriers.

The Seebeck coefficient's general negative value is compatible with degenerate semiconducting or metallic behavior, in which transport is dominated by electrons. Multi-valley conduction bands or complex band structure effects are marked by the non-monotonic behavior, which consists of a dip followed by a sharp upswing. The material retains adequate carrier energy filtration, which is advantageous for thermoelectric applications, as seen by the blasting increase in the Seebeck coefficient's magnitude.

The presence of a local minimum (in absolute value) at low temperatures might suggest:

- Transition in **scattering mechanisms**.
- The onset of **band convergence** or change in the **DOS slope** near the Fermi level.
- At high temperatures (e.g., −40 to −45 μV/K at >1200 K), this material exhibits a moderate S. This is fairly low for ordinary semiconducting thermoelectric materials, but it might potentially contribute if σ is very high and κ is low. High thermal losses may pose a constraint for the ZT unless alloying, nanostructuring, or defect inclusion are used to engineer or lower lattice thermal conductivity.
  At high temperatures, the material shows n-type conduction as it gains thermopower, according to the temperature-dependent Seebeck coefficient. The steady rise indicates possibilities for high-temperature thermoelectric applications, in particular when paired with band engineering and thermal conductivity suppression techniques, even though the absolute values of S are moderate (maxing at about 45 μV/K).
-

Power factor

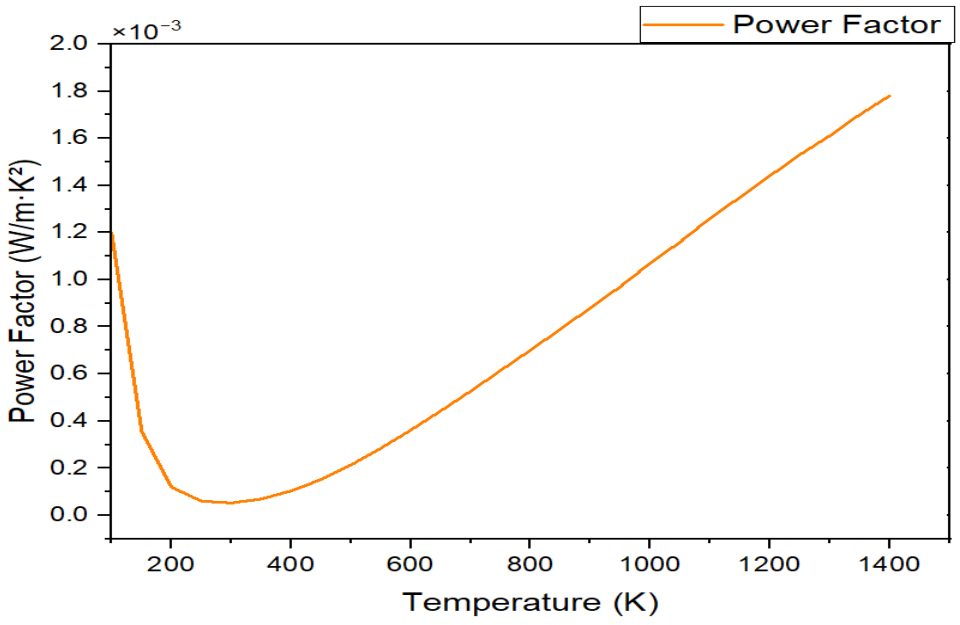


Fig. 17: *Calculated power factor for a range of temperature*

- **200–300 K**:
  The power factor **drops steeply**, reaching a **local minimum**. This drop corresponds with the lowest values of the Seebeck coefficient and a declining trend in electrical conductivity.
- **300–1400 K**:
  There is a **steady and almost exponential increase** in the power factor, reaching a peak value of nearly **1.8 × 10⁻³ W/m·K²** at high temperatures (~1400 K).

This strong upward trend implies a **favourable thermoelectric response at elevated temperatures**.

The maximum observed power factor value of **1.8 × 10^{-3} W/m·K^2** is **modest** in comparison to state-of-the-art thermoelectric materials (such as Bi_2Te_3 or PbTe, which can exceed **4–6 × 10^{-3} W/m·K^2**), but still respectable, especially if $CuLuO_3$ has a **low thermal conductivity**.

Combined with the earlier thermal and electrical data:

- Thermal conductivity was seen to **increase with temperature** (which is a limiting factor),
- Electrical conductivity remained high and stable, and
- The Seebeck coefficient increased linearly at high temperatures,

this rising power factor suggests $CuLuO_3$ has good electronic transport characteristics, even if phonon transport (heat) needs optimization

Strategy for Improvement

To make $CuLuO_3$ a more competitive thermoelectric material, strategies could include:

- **Doping or alloying** to optimize carrier concentration and further increase S without compromising σ,
- **Nanostructuring** or introducing **point defects** to reduce lattice thermal conductivity,
- **Strain engineering** or using **superlattices** to tune the band structure for enhanced thermoelectric properties.

Stability in perovskite

The stability of perovskite materials is a central concern in both experimental and theoretical research, especially when exploring novel perovskites for thermoelectric applications. Theoretical investigations must grapple with a range of intrinsic and extrinsic instability mechanisms, which can critically impact the predicted and real-world performance of these materials.

Intrinsic Stability Issues

Thermodynamic and Phase Stability

- The thermodynamic phase stability of perovskites determines their synthesizability and resistance to decomposition under operational conditions. Theoretical approaches often use Density Functional Theory (DFT) to calculate the energy above the convex hull (Ehull) as a measure of phase stability. However, DFT calculations are computationally expensive for high-throughput screening, leading to the adoption of machine learning (ML) models trained on DFT data to predict stability across large chemical spaces[95].
- The Goldschmidt tolerance factor is a traditional metric for predicting the formability and stability of perovskite structures, but deviations can lead to unwanted phases or instability at operational temperatures.

Ion Migration and Defect Chemistry

- Ion migration, especially of halide ions and organic cations, is a significant cause of instability. It can lead to phase segregation, defect formation, and dynamic changes in electronic and thermal properties, all of which are detrimental to thermoelectric performance[79].
- Theoretical studies must model defect formation energies and migration barriers, often using DFT and molecular dynamics (MD) simulations, but these calculations are sensitive to the chosen parameters and may not capture all real-world complexities [74].

Structural Dynamics

- Perovskite structures can undergo phase transitions (e.g., orthorhombic to tetragonal to cubic) as a function of temperature, which affects their stability and transport properties. MD simulations are used to study these transitions and the associated vibrational spectra, but the results depend heavily on the accuracy of force fields and input parameters [74].

Extrinsic factor

Environmental Sensitivity

- Perovskites are highly sensitive to moisture, oxygen, and light (especially UV), leading to rapid degradation through hydrolysis or photochemical reactions. Theoretical models must account for these extrinsic factors, often by simulating surface reactions or environmental exposure, but this remains a complex and evolving field 93.
- Encapsulation can mitigate some environmental effects, but for thermoelectric devices operating at elevated temperatures, moisture and oxygen ingress remain critical concerns93.

Thermal Instability

- Many perovskites decompose at relatively low temperatures (as low as 85–100°C), forming lead iodide and other byproducts. This limits their operational window for thermoelectric applications, which often require sustained performance at higher temperatures 93.
- Theoretical predictions of thermal stability involve calculating decomposition pathways, reaction energies, and kinetic barriers, but these require accurate thermodynamic and kinetic data, which are not always available 81.

Interface and Device Instability

- The interfaces between perovskite layers and charge transport materials (e.g., electron or hole transport layers) are prone to chemical reactions, defect formation, and interdiffusion, all of which can accelerate degradation. Theoretical modeling of these interfaces is complex but essential for realistic stability predictions92.
- Additives, dopants, and surface treatments can improve stability, but their effects must be understood and optimized through both experimental and computational studies 91.

Stability Assessment Methodologies for Perovskite Materials

Theoretical investigations of perovskite stability for thermoelectric applications rely on three principal methodologies: the Goldschmidt tolerance factor for structural compatibility prediction, phonon dispersion calculations for dynamical stability analysis, and *ab initio* molecular dynamics (AIMD) for simulating degradation pathways under operational conditions. These approaches address distinct aspects of stabilitystructural integrity, vibrational modes, and time-dependent atomic behaviorwhile complementing one another in guiding material design. Recent advancements in computational tools and machine learning integration have enhanced the accuracy and efficiency of these methods, though challenges persist in reconciling theoretical predictions with experimental observations under complex thermoelectric operating environments78 77.

Structural Stability Assessment via Goldschmidt Tolerance Factor

The **Goldschmidt tolerance factor** (t) remains a foundational tool for predicting perovskite formability. Defined as:

$$t = \frac{r_A + r_X}{\sqrt{2}(r_B + r_X)}$$

where rA, rB, and rX are the ionic radii of the A-site cation, B-site cation, and anion, respectively80. Values 0.9<t<1 indicate ideal cubic perovskite structures, while deviations lead to non-perovskite phases (e.g., hexagonal or orthorhombic). For instance, $BaTiO_3$ exhibits t=1.06 , explaining its tetragonal distortion.

Limitations and Modifications

While effective for oxides, the classical ttt fails for hybrid perovskites due to anisotropic organic cations (e.g., methylammonium). Modified versions, such as the **Bartel tolerance factor** (t′), incorporate electronegativity differences (Δχ):

$$t' = t(1 - \alpha\, \Delta\chi_{X-A})$$

- $\Delta\chi_{X-A}$ represents the electronegativity difference between the **A-site** and **X-site** elements in the perovskite structure.
- t is the standard tolerance factor.
- α is an empirical scaling factor.

where α is an empirical parameter. This adjustment improves predictions for halide perovskites like $MAPbI_3$, where $t'>1.03$ correlates with phase instability [79].

Dynamical Stability using Phonon Dispersion Calculations

Methodology and Computational Workflow

Phonon dispersion spectra, derived from **density functional perturbation theory (DFPT)** or the **direct method**, reveal vibrational stability by identifying imaginary frequencies (soft modes) [81] . Key steps include:

1. **Supercell optimization**: Using DFT to minimize energy (e.g., Quantum ESPRESSO).
2. **Force constant extraction**: Displacing atoms and calculating Hellmann-Feynman forces.
3. **Dynamical matrix diagonalization**: Yielding phonon frequencies across the Brillouin zone[81][.
   For example, $CsSnCl_3$ exhibits imaginary frequencies at the Γ-point, indicating dynamical instability in its cubic phase [82].

Case Studies and Challenges

- **$MAPbI_3$**: Phonon spectra show soft modes below 50 cm^{-1}, linked to low thermal conductivity (~0.5 W/m·K) but also phase segregation under thermal stress[83].
- **$SrTiO_3$**: Calculated longitudinal optical (LO)-transverse optical (TO) splitting matches inelastic X-ray scattering data, validating DFPT for oxide perovskites[84]. Limitations arise from finite supercell sizes and anharmonic effects at high temperatures. Hybrid DFPT-AIMD methods now address anharmonicity by integrating temperature-dependent force constants [84].

Degradation Pathways via Ab Initio Molecular Dynamics (AIMD)

Simulating Operational Conditions

AIMD tracks atomic trajectories under finite temperatures (300–1500 K) and external stimuli (moisture, light), providing insights into:

1. **Thermal decomposition**: E.g., $MAPbI_3$ decomposes via Pb-I bond breaking at 85°C, forming PbI_2 and volatile CH_3NH_2 85.
2. **Moisture-induced degradation**: Water intercalation at perovskite surfaces (e.g., RP-phase 2D perovskites) forms hydrated intermediates, accelerating ion migration 86.

Advancements in Sampling and Accuracy

- **Machine learning potentials**: Neural network models trained on AIMD data reduce computational cost by 90% while preserving fidelity 87.
- **Metadynamics**: Enhanced sampling techniques map free-energy landscapes for degradation reactions, identifying critical barriers (e.g., 0.8 eV for I_2 formation in $CsPbI_3$)88.

Challenges in Timescale Bridging

AIMD simulations (~100 ps) struggle to capture slow degradation processes (e.g., phase segregation over hours). Coarse-grained models and kinetic Monte Carlo methods are being integrated to address this gap 89.

Comparative Analysis of Methodologies

Method	Strengths	Limitations	Thermoelectric Relevance
Goldschmidt	Rapid screening, intuitive design rules	Ignores temperature, defects, kinetics	Guides initial compositional selection
Phonon dispersion	Quantifies dynamical stability, anharmonicity	Computationally intensive, limited to 0 K	Predicts thermal conductivity and phase transitions
AIMD	Real-time degradation modelling	Timescale restrictions, high resource cost	Evaluates operational lifetime under stress

TABLE 3: *Comparative Analysis of Computational Methods for Thermoelectric Material Evaluation*